

國立交通大學

電信工程學系碩士班 碩士論文

多輸入多輸出無線通訊中基於 QR 分解
逐級偵測之最小錯誤率功率分配法

BER-Minimized Power Allocation
for QR-Based Successive Detection
in MIMO Wireless Communications

研究生：匡劼剛

Student: Jie-Gang Kuang

指導教授：李大嵩 博士

Advisor: Dr. Ta-Sung Lee

中華民國九十六年十月

多輸入多輸出無線通訊中基於 QR 分解逐級偵測之
最小錯誤率功率分配法

BER-Minimized Power Allocation for QR-Based
Successive Detection in MIMO Wireless Communications

研究生：匡劼剛

Student: Jie-Gang Kuang

指導教授：李大嵩 博士

Advisor: Dr. Ta-Sung Lee

國立交通大學

電信工程學系碩士班

碩士論文

A Thesis

Submitted to Department of Communication Engineering
College of Electrical and Computer Engineering

National Chiao Tung University

in Partial Fulfillment of the Requirements

for the Degree of

Master of Science

in

Communication Engineering

October 2007

Hsinchu, Taiwan, Republic of China

中華民國九十六年十月

多輸入多輸出無線通訊中基於 QR 分解逐級偵測 之最小錯誤率功率分配法

學生：匡劼剛

指導教授：李大嵩 博士

國立交通大學電信工程學系碩士班

摘要

新一代無線通訊中，空間多工（Spatial Multiplexing）和傳送多樣（Transmit Diversity）為廣受矚目的技術。在本論文中，吾人考慮空間多工系統搭配基於 QR 分解逐級偵測技術，提出一種最小錯誤率之功率分配法。吾人設計的方法是利用空間多工下 QR 分解的機率分布，針對降低整體通道的平均錯誤率做功率分配，可在中高訊號雜訊比的情況下改善系統的效能表現。此外透過雙重空時傳送多樣（Double Space-Time Transmit Diversity）下 QR 分解的機率分布，吾人提出的功率分配法亦可適用於雙重空間傳送多樣系統。儘管雙重空間傳送多樣系統中部份機率分布為估計得來，其平均錯誤率之公式仍相當準確。模擬結果顯示，吾人提出的方法應用在雙重空間傳送多樣系統時，亦可在中高訊號與雜訊比的環境中改善無線通訊系統效能。此外，電腦模擬顯示，吾人設計的功率分配法可延伸用在多重空間傳送多樣系統中。

BER-Minimized Power Allocation for QR-Based Successive Detection in MIMO Wireless Communications


Student: Jie-Gang Kuang

Advisor: Dr. Ta-Sung Lee

Department of Communication Engineering

National Chiao Tung University

Abstract

The logo of National Chiao Tung University is a circular emblem. It features a gear-like outer border. Inside, there are stylized representations of books and a graduation cap. The year '1896' is inscribed at the bottom of the inner circle.

It is well known that spatial multiplexing and transmit diversity are popular techniques in modern wireless communications. In this thesis, we first propose a BER-minimized power allocation strategy for spatial multiplexing systems over i.i.d. Rayleigh fading channels based on the QR-based successive detection scheme. With the knowledge of distribution of QR decomposition in spatial multiplexing, the design criterion for power loading is the overall BER averaged with respect to the channel distribution. Based on the closed-form solution, the optimal power allocation scheme is proposed, which aims to minimize the overall average BER performance of spatial multiplexing systems at medium-to-high SNR. Afterwards, with the distribution of the R matrix of QR decomposition for DSTTD systems, the design procedure of the power allocation scheme proposed for spatial multiplexing systems can be applied to DSTTD systems. Although parts of the distribution of the R matrix in DSTTD are merely approximations, the estimated average BERs are quite accurate. The power allocation scheme adapted for DSTTD systems are shown to be also effective at the high SNR regime by numerical simulations. Moreover, the proposed scheme can be further extended to multiple STTD systems.

Acknowledgement

I would like to express my deepest gratitude towards my advisor, Dr. Ta-Sung Lee, for his enthusiastic guidance and great patience. His positive attitude has guided me in many areas and has propelled me in the direction of reaching my future goals. In addition, I would like to express many heartfelt thanks to all the members and staff of the Communication System Design and Signal Processing (CSDSP) Lab for their constant support and encouragement. Last but not least, I would like to show my most sincere appreciation and love to my family for their continual love and support of my pursuit of excellence. Thank you once again.



Contents

Chinese Abstract.....	I
English Abstract.....	II
Acknowledgement.....	III
Contents	IV
List of Figures	VII
Acronym Glossary.....	IX
Notations	XI
Chapter 1 Introduction.....	1
Chapter 2 Model of MIMO Wireless Communication Systems....	4
2.1 Review of Spatial Multiplexing	4
2.2 Review of Double Space-Time Transmit Diversity	6
2.2.1 Alamouti Space-Time Transmit Diversity	7
2.2.2 Double Space-Time Transmit Diversity Systems	9
2.3 QR Decomposition of Channel Matrix	11
2.3.1 Review of QR Decomposition.....	11
2.3.2 QR Decomposition of Channel Matrix in Spatial Multiplexing MIMO Systems	12
2.3.3 QR Decomposition of Channel Matrix in Double Space-Time	

Transmit Diversity Systems.....	13
2.4 Model of MIMO Wireless Communication Systems with QR-Based Successive Detection	16
2.4.1 Model of Spatial Multiplexing MIMO systems	16
2.4.2 Model of Double Space-Time Transmit Diversity Systems	18
2.5 Computer Simulations.....	19
2.6 Summary	22
 Chapter 3 Power Allocation for Minimum BER in Spatial Multiplexing Systems	23
3.1 Bound for BER of QR-Based Successive Detection	24
3.2 Optimal Power Allocation for Minimum Upper Bound of Overall Average BER.....	29
3.3 Computer Simulations.....	33
3.4 Summary	36
 Chapter 4 Power Allocation for Minimum BER in Double Space-Time Transmit Diversity Systems	37
4.1 Distribution of Diagonal Elements of R Matrix in QR Decomposition.....	38
4.2 Optimal Power Allocation for Minimum Upper Bound of Overall Average BER.....	43
4.3 Extension of Proposed Optimal Power Allocation Scheme	48
4.4 Computer Simulations.....	50
4.5 Summary	54
 Chapter 5 Conclusion	55

Appendix A Proof of Lemma 2.4 57

Bibliography 62



List of Figures

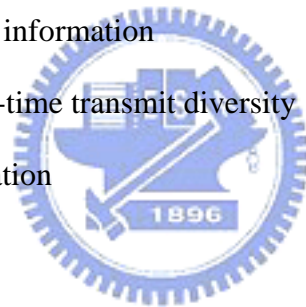
Figure 2.1: Block diagram of a spatial multiplexing system with n_T transmit antennas and n_R receive antennas	6
Figure 2.2: Block diagram of an Alamouti space-time coded system for two transmit antennas and single receive antenna	9
Figure 2.3: Block diagram of a DSTTD system with four transmit antennas and two receive antennas	11
Figure 2.4: Average BER performances of spatial multiplexing MIMO systems with different receivers with QPSK modulation	21
Figure 2.5: Average BER performances of DSTTD systems with different receivers with QPSK modulation	21
Figure 3.1: Block diagram of a 4×4 spatial multiplexing MIMO system with the QR receiver with the transmit power allocation scheme	25
Figure 3.2: Evaluations of upper bounds for the lower bound of overall average BER in 4×4 spatial multiplexing systems with the QR receiver with QPSK modulation.....	34
Figure 3.3: Average BER performances of 4×4 spatial multiplexing systems with different receivers with QPSK modulation	35
Figure 3.4: Average BER performances of 4×4 spatial multiplexing systems with the QR receivers with different modulation orders.....	35
Figure 4.1: Comparison between the sampled data of $2 R_{33} ^2$ and the gamma pdf with $k = 2$ and $\theta = 2$	42
Figure 4.2: Block diagram of a DSTTD system with the QR receiver with transmit power allocation scheme	44
Figure 4.3: Comparisons between $2 R_{33} ^2$, $2 R_{55} ^2$ and the gamma pdfs with $k = 4$,	

$\theta = 2$, and $k = 2$, $\theta = 2$, respectively	49
Figure 4.4: Evaluations of upper bounds for the lower bound of average overall BER in DSTTD systems with QPSK modulation.....	52
Figure 4.5: Average BER performances of DSTTD systems with different receivers with QPSK modulation	52
Figure 4.6: Average BER performances of DSTTD systems with the QR receiver with different modulation orders	53
Figure 4.7: Average BER performances of triple STTD systems with the QR receiver	53

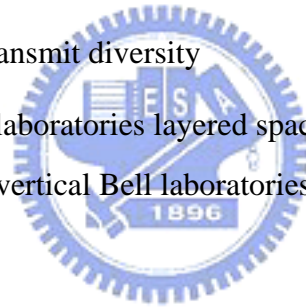


Acronym Glossary

AWGN	additive white Gaussian noise
BER	bit error rate
BLAST	Bell laboratories layered space-time
BPSK	binary phase shift keying
BS	base station
CIR	channel impulse response
CSI	channel state information
DSTTD	double space-time transmit diversity
EP	error propagation
EQ	equalizer
IEEE	institute of electrical and electronics engineers
ISI	intersymbol interference
LB	lower bound
LOS	line of sight
MIMO	multiple-input multiple-output
MISO	multiple-input single-output
ML	maximum likelihood
MMSE	minimum mean-square error
MRC	maximal ratio combining
MS	mobile station
MU	multi-user

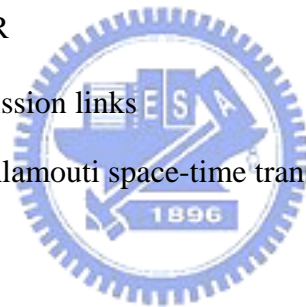


OSTBC	orthogonal space-time block code
PL	power loading
QAM	quadrature amplitude modulation
QPSK	quadrature phase shift keying
SDMA	spatial division multiple access
SIMO	single-input multiple-output
SISO	single-input single-output
SM	spatial multiplexing
SNR	signal-to-noise ratio
SIC	successive interference cancellation
STBC	space-time block code
STTD	space-time transmit diversity
V-BLAST	vertical Bell laboratories layered space-time
ZF-VBLAST	zero-forcing vertical Bell laboratories layered space-time



Notations

E_s	symbol energy
n_T	number of transmit antennas
n_R	number of receive antennas
N_0	noise power spectrum density
R	rate of space-time codes
\mathbf{P}	power loading matrix
ρ	instantaneous SNR
M	number of transmission links
η	receive SNR for Alamouti space-time transmit diversity



Chapter 1

Introduction

Multiple-input multiple-output (MIMO) systems, employing several transmit and receive antennas at both ends, are capable of providing a significant increase in capacity compared to traditional single-input single-output (SISO) systems [1], [2]. The spatial multiplexing technique was proposed to increase system capacity. On the other hand, orthogonal space-time code designs [3], [4] generally yield good bit error rate (BER) performance. Space-time transmit diversity (STTD) as well as Alamouti space-time block codes (STBCs) was introduced to provide transmit diversity gain. One main limitation of these schemes providing transmit diversity is that they do not achieve full rate, which, for a single channel, means that each transmitter antenna transmits one symbol per second per Hertz. To exploit these two advantages at the same time, double space-time transmit diversity (DSTTD) with four antennas was suggested in [5], [6]. In this system, two STTD encoders are used at the transmitter and interference cancellation based detector is employed at the receiver.

When the transmitter has acquired some knowledge of the channel state information (CSI), a precoder can be applied at the transmitter to improve the performance of the system. With full knowledge of CSI, a minimum mean-square error (MMSE) precoder has been designed in [8]. To reduce the requirement of CSI feedback, a diagonal precoder was suggested in [9] for Vertical Bell Laboratories Layered

Space-Time (V-BLAST) detection [16]. The design adjusts the power and rate of each antenna to minimize either the maximum BER of all sub-streams or the total transmission power. However, when the transmission rates in the antennas are equal, this may lead to the result of equal power allocation.

This thesis addresses the symbol detection problem of spatial multiplexing MIMO systems and DSTTD systems over i.i.d. Rayleigh fading channels. To achieve the BER performance balance between linear receivers and joint maximum likelihood (ML) detection, a QR-based successive symbol detection scheme with proper symbol power allocation is proposed. There have been many performance measures for successive symbol recovery in spatial multiplexing systems and DSTTD systems discussed in [9]-[15]. The average BER with error free front-layer decision feedback, though just a lower bound of the exact mean error rate, is simple to characterize and, furthermore, is closely related to the upper bound of the block error rate when error propagation occurs [15]. Thus, it becomes an efficient and meaningful performance metric accounting for the actual BER performance analysis. Motivated by this fact and to also guarantee the performance improvements regardless of the instantaneous channel conditions, a power allocation scheme aiming to minimizing the overall BER averaged with respect to the channel distribution is proposed. Specific contributions of this thesis include:

1. By exploiting the distinctive channel matrix structure induced by DSTTD, we derive an explicit formula for the associated QR decomposition.
2. With the approved statistical property of the R matrix in QR decomposition for spatial multiplexing systems and DSTTD systems, the closed-form upper bounds for the BER metric are obtained.
3. By minimizing the upper bounds, an optimal power allocation scheme is proposed, and is obtained through numerical search.

Although performance improvement of the QR receiver via symbol power loading

has been addressed in many previous researches [9]-[16], all of them are based on a given fixed channel realization known to the transmitter. The strategy proposed in this thesis is grounded on the overall BER averaged over the channel distribution; that is, it is independent of the instantaneous channel condition, and thus requires fewer feedback messages from the receiver. Furthermore, the distribution of QR decomposition for DSTTD is discovered. This makes it possible to apply the design criterion to DSTTD systems, and even multiple STTD systems.

This thesis is organized as follows. In Chapter 2, the review of spatial multiplexing MIMO systems and DSTTD systems is introduced, and the statistical property and particular matrix structure of QR decompositions for spatial multiplexing and DSTTD are stated. Additionally, the system models of spatial multiplexing and DSTTD with QR-based successive detection are also built. In Chapter 3, with knowledge of distribution of the R matrix for spatial multiplexing, a power allocation scheme which aims to minimize the overall average BER performance of spatial multiplexing systems is proposed. In Chapter 4, the probability density functions (pdfs) of the matrix for DSTTD systems are calculated and estimated. With the exact and approximated pdfs, the power loading factors proposed for DSTTD systems are obtained. Computer simulations of BER performances of the proposed scheme are then illustrated. Finally, we conclude this thesis and describe some potential future works in Chapter 5.

Chapter 2

Model of MIMO Wireless Communication Systems

This chapter first presents the review of spatial multiplexing (SM) and double space-time transmit diversity (DSTTD). Spatial multiplexing scheme is a promising technique to enhance data rate, and it can only be implemented in multiple-input multiple-output (MIMO) systems. Before the review of DSTTD systems, we will give an introduction to Alamouti space-time transmit diversity. DSTTD system is basically a simple combination of spatial multiplexing and space-time transmit diversity such that both capacity and reliability can be achieved simultaneously. Afterwards, we will review the QR decomposition and introduce the QR decompositions of spatial multiplexing systems and DSTTD systems. We detect the received symbols by exploiting these special structures and compare their performances with the conventional detection methods.

2.1 Review of Spatial Multiplexing

Spatial multiplexing is capable of offering a linear increase in the transmission rate (or capacity) for the same bandwidth and without additional power consumption. The improvement is proportional to the number of transmit-receive antenna pairs or the

minimum of number of transmit antennas and that of receive antennas. The bit stream to be transmitted is divided into multiple sub-streams, modulated and transmitted simultaneously from each transmit antenna [1]. Under favorable channel conditions, the spatial signatures of these signals induced at the receive antennas can be well separated. The receiver, having knowledge of the channels, is able to differentiate among the co-channel signals and extract all signals, after which demodulation yields the original sub-streams that can now be combined to give the original bit stream. Spatial multiplexing can also be applied in a multi-user format (MIMO-MU, also known as space division multiple access or SDMA).

We assume that in spatial multiplexing MIMO systems there are n_T transmit antennas at transmitter and n_R receive antennas at receiver. The channel response from transmit antenna j to receive antenna i , h_{ij} , is assumed flat and can be modeled as an i.i.d. complex zero-mean Gaussian variable with unit variance. Let x_i be the symbol to be transmitted from antenna i , and the received signal on receive antenna j , y_j , is given by

$$y_j = h_{1j}x_1 + h_{2j}x_2 + \cdots + h_{n_T j}x_{n_T}. \quad (2.1)$$

Accordingly, we can express the spatial multiplexing MIMO systems in matrix form:

$$\mathbf{y} = \begin{bmatrix} y_1 \\ y_2 \\ \vdots \\ y_{n_R} \end{bmatrix} = \begin{bmatrix} h_{11} & h_{12} & \cdots & h_{1n_T} \\ h_{21} & h_{22} & \cdots & h_{2n_T} \\ \vdots & \vdots & \ddots & \vdots \\ h_{n_R 1} & h_{n_R 2} & \cdots & h_{n_R n_T} \end{bmatrix} \begin{bmatrix} x_1 \\ x_2 \\ \vdots \\ x_{n_T} \end{bmatrix} + \begin{bmatrix} n_1 \\ n_2 \\ \vdots \\ n_{n_R} \end{bmatrix} = \mathbf{H}\mathbf{x} + \mathbf{n}, \quad (2.2)$$

where n_i ($i=1, 2, \dots, n_R$) are i.i.d. complex Gaussian random variables with zero mean and variance 1.

A simple block diagram is shown in Figure 2.1. The data stream to be transmitted

is demultiplexed into n_T sub-streams which are transmitted simultaneously. At receiver, the received data stream is obtained by combining the detected received signals. Although spatial multiplexing technique is capable of providing a boost in transmission data rate, it can not induce diversity gain to improve the reliability of wireless communication systems. Therefore, we will discuss transmit diversity technique in the next section and give a simple transmission scheme to enhance the reliability of wireless communication systems.

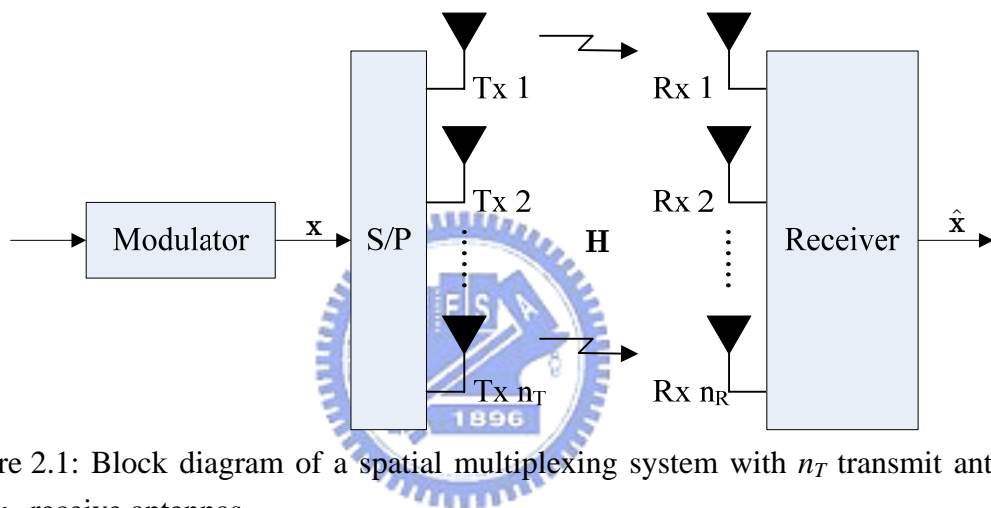


Figure 2.1: Block diagram of a spatial multiplexing system with n_T transmit antennas and n_R receive antennas

2.2 Review of Double Space-Time Transmit

Diversity

Recently space-time transmit diversity (STTD) has been studied extensively as a method of combating detrimental effects in wireless fading channels because of its relative simplicity of implementation and feasibility of having multiple antennas at the base station. The first bandwidth efficient transmit diversity scheme was proposed by Wittneben [17], and it includes the delay diversity scheme of Seshadri and Winters [18] as a special case. More recently, space-time trellis coding has been proposed [3] which

combines signal processing at the receiver with coding techniques appropriate to multiple transmit antennas and provides significant gain over [17] and [18]. In addressing the issue of decoding complexity, Alamouti discovered a remarkable transmission scheme which can provide full rate and full diversity gain with two transmit antennas [4].

2.2.1 Alamouti Space-Time Transmit Diversity

In the Alamouti space-time transmit diversity scheme, we consider two antennas at the transmitter and a single receive antenna. Assume that an M -ary modulation is used and each group of m information bits is modulated, where $m = \log_2 M$. The symbols to be space-time encoded are divided into groups of two symbols in each encoding operation. Two different symbols x_1 and x_2 in each group are transmitted simultaneously from antennas 1 and 2 respectively during the first symbol period. During the next symbol period, x_2^* is transmitted from antenna 1 and $-x_1^*$ is transmitted from antenna 2. Superscripts $(\cdot)^T$, $(\cdot)^*$, and $(\cdot)^H$ denote transpose, complex conjugate, and Hermitian operation, respectively.

We assume that the channel remains constant over the two symbol periods, and is frequency flat. Let h_1 and h_2 be the fading channel coefficients from antenna 1 and antenna 2. The real part and imaginary part of channel coefficients are modeled as Gaussian random variables with zero mean and variance 0.5. Consequently, $\mathbf{h} = [h_1 \ h_2]^T$ and the signals y_1 and y_2 received over the two symbol periods are given by

$$y_1 = h_1 x_1 + h_2 x_2 + n_1, \quad (2.3)$$

$$y_2 = h_1 x_2^* - h_2 x_1^* + n_2, \quad (2.4)$$

where n_1 and n_2 are i.i.d. complex Gaussian random variables with zero mean. The real part and imaginary part of noise have the same variance $n_T/(2SNR)$, where SNR stands for the average signal-to-noise ratio. The received signals can be written as

$$\begin{bmatrix} y_1 \\ y_2 \end{bmatrix} = \begin{bmatrix} x_1 & x_2 \\ x_2^* & -x_1^* \end{bmatrix} \begin{bmatrix} h_1 \\ h_2 \end{bmatrix} + \begin{bmatrix} n_1 \\ n_2 \end{bmatrix}, \quad (2.5)$$

and we can obtain a rearranged signal vector \mathbf{y} as follows:

$$\mathbf{y} = \begin{bmatrix} y_1 \\ y_2^* \end{bmatrix} = \begin{bmatrix} h_1 & h_2 \\ -h_2^* & h_1^* \end{bmatrix} \begin{bmatrix} x_1 \\ x_2 \end{bmatrix} + \begin{bmatrix} n_1 \\ n_2^* \end{bmatrix} = \mathbf{H}\mathbf{x} + \mathbf{n}. \quad (2.6)$$

The channel matrix \mathbf{H} is orthogonal (i.e., $\mathbf{H}^H \mathbf{H} = \|\mathbf{h}\|_F^2 \mathbf{I}_2$). If $\mathbf{z} = \mathbf{H}^H \mathbf{y}$, we can get

$$\mathbf{z} = \mathbf{H}^H \mathbf{H}\mathbf{x} + \mathbf{H}^H \mathbf{n} = \|\mathbf{h}\|_F^2 \mathbf{I}_2 \mathbf{x} + \tilde{\mathbf{n}}, \quad (2.7)$$

where $E\{\tilde{\mathbf{n}}\} = \mathbf{0}_{2,1}$ and $E\{\tilde{\mathbf{n}}\tilde{\mathbf{n}}^H\} = \|\mathbf{h}\|_F^2 N_0 \mathbf{I}_2$. Hence, the effective channel for symbols x_i ($i = 1, 2$) becomes

$$z_i = \|\mathbf{h}\|_F^2 x_i + \tilde{n}_i, \quad i = 1, 2, \quad (2.8)$$

and the receive SNR, η , per symbol is given by

$$\eta = \frac{\|\mathbf{h}\|_F^2 \rho}{2}, \quad (2.9)$$

where $\rho \triangleq E_s/N_0$ is the average signal-to-noise ratio (SNR).

The block diagram that includes modulator, serial to parallel structure and Alamouti space-time encoder is shown in Figure 2.2. The data stream is demultiplexed

into two sub-streams which are converted from serial to parallel and mapped to an Alamouti encoder. The Alamouti scheme extracts a diversity order of 2 (full n_T diversity), even in the absence of channel knowledge at the transmitter.

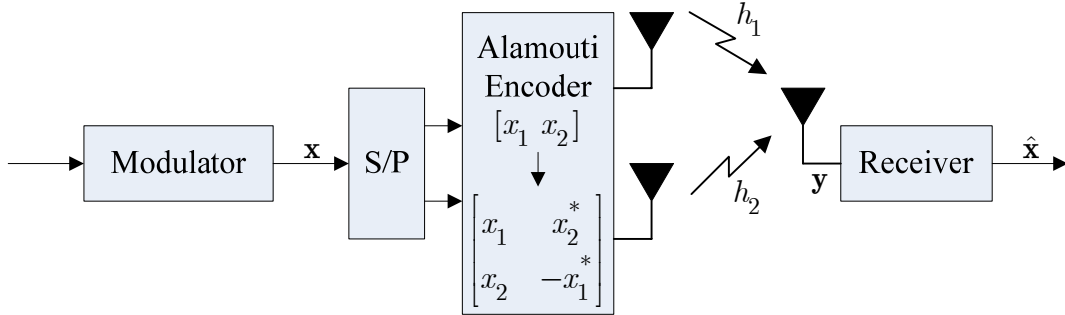


Figure 2.2: Block diagram of an Alamouti space-time coded system for two transmit antennas and single receive antenna

2.2.2 Double Space-Time Transmit Diversity Systems

After the review of Alamouti space-time transmit diversity, combining spatial multiplexing technique with it, we then introduce the concept of double space-time transmit diversity (DSTTD) systems. The DSTTD system is an open-loop multiple-input multiple-output system with four transmit antennas and two receive antennas. It has two Alamouti space-time encoders at transmitter and obtains high data rate as well as transmit diversity.

In DSTTD system, four symbols $\{x_1, x_2, x_3, x_4\}$ are transmitted during two symbol periods. The symbols are first arranged into two groups $\{x_1, x_2\}$ and $\{x_3, x_4\}$, and they are then mapped into two Alamouti space-time encoders respectively. Let h_{ij} be the channel coefficient from transmit antenna j to receive antenna i , and it is complex Gaussian with zero mean and unit variance. At receiver

antenna 1, the received signals $[y_{1,1} \ y_{1,2}]^T$ during two symbol periods can therefore be written in matrix form as

$$\begin{bmatrix} y_{1,1} \\ y_{1,2} \end{bmatrix} = \begin{bmatrix} x_1 & x_2 & x_3 & x_4 \\ x_2^* & -x_1^* & x_4^* & -x_3^* \end{bmatrix} \begin{bmatrix} h_{11} \\ h_{12} \\ h_{13} \\ h_{14} \end{bmatrix} + \begin{bmatrix} n_{1,1} \\ n_{1,2} \end{bmatrix}, \quad (2.10)$$

where $n_{i,t}$ is noise on receive antenna i at symbol period t , which is assumed complex zero-mean Gaussian with variance 1. We can express $[y_{2,1} \ y_{2,2}]^T$ with similar formulation:

$$\begin{bmatrix} y_{2,1} \\ y_{2,2} \end{bmatrix} = \begin{bmatrix} x_1 & x_2 & x_3 & x_4 \\ x_2^* & -x_1^* & x_4^* & -x_3^* \end{bmatrix} \begin{bmatrix} h_{21} \\ h_{22} \\ h_{23} \\ h_{24} \end{bmatrix} + \begin{bmatrix} n_{2,1} \\ n_{2,2} \end{bmatrix}. \quad (2.11)$$

Combining (2.10) and (2.11), we can rearrange the received signals as follows:

$$\mathbf{y} = \begin{bmatrix} \mathbf{y}_1 \\ \mathbf{y}_2 \end{bmatrix} = \begin{bmatrix} y_{1,1} \\ y_{1,2} \\ y_{2,1} \\ y_{2,2} \end{bmatrix} = \begin{bmatrix} h_{11} & h_{12} & h_{13} & h_{14} \\ -h_{12}^* & h_{11}^* & -h_{14}^* & h_{13}^* \\ h_{21} & h_{22} & h_{23} & h_{24} \\ -h_{22}^* & h_{21}^* & -h_{24}^* & h_{23}^* \end{bmatrix} \begin{bmatrix} x_1 \\ x_2 \\ x_3 \\ x_4 \end{bmatrix} + \begin{bmatrix} n_{1,1} \\ n_{1,2} \\ n_{2,1} \\ n_{2,2} \end{bmatrix} = \mathbf{H}\mathbf{x} + \tilde{\mathbf{n}}. \quad (2.12)$$

The block diagram of a DSTTD system with four transmit antennas and two receive antennas is shown in Figure 2.3. The data stream is demultiplexed into four sub-streams which are divided into two groups. Each group of two sub-streams is encoded by an Alamouti space-time encoder.

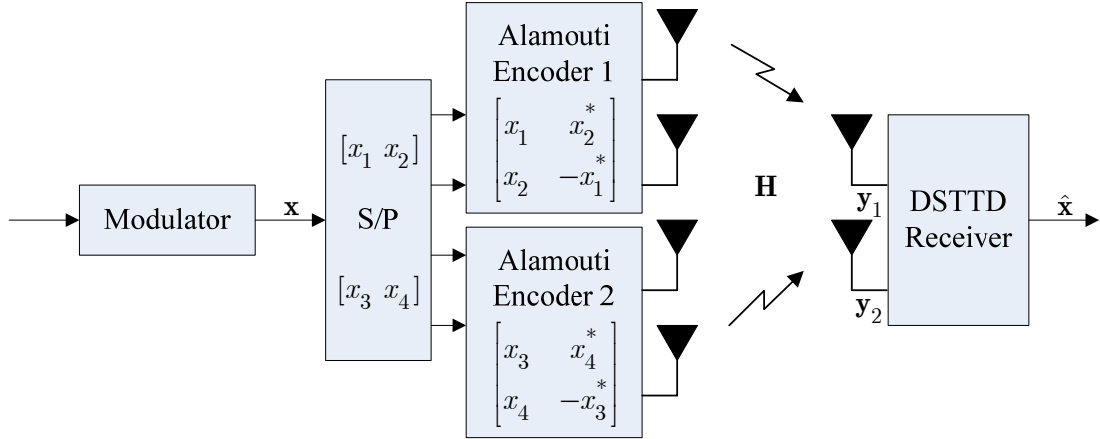


Figure 2.3: Block diagram of a DSTTD system with four transmit antennas and two receive antennas

2.3 QR Decomposition of Channel Matrix

In this section, we will introduce the QR decompositions of spatial multiplexing MIMO systems and double space-time transmit diversity systems. The diagonal entries of \mathbf{R} for spatial multiplexing systems are related to chi-square distribution, and this let us be able to find a performance bound of spatial multiplexing systems. For QR decomposition of DSTTD systems \mathbf{R} has a special structure, and the diagonal entries of it are found to be associated with the entries of the DSTTD channel matrix.

2.3.1 Review of QR Decomposition

QR decomposition is one of the well-known decompositions, and can be obtained by the Gram-Schmidt process straightforwardly. We know that the formulation of Gram-Schmidt procedure is to find an orthonormal basis for the space spanned by the original linearly independent basis. The Gram-Schmidt process frequently appears in the matrix form, and it is equivalent to QR decomposition. Let us show the lemma of QR decomposition and apply it to spatial multiplexing MIMO systems and double

space-time transmit diversity systems.

Lemma 2.1: Every matrix $\mathbf{H}_{m \times n}$ with linearly independent columns can be uniquely factored as $\mathbf{H} = \mathbf{Q}\mathbf{R}$ in which the columns of $\mathbf{Q}_{m \times n}$ are an orthonormal basis for $R(\mathbf{H})$ and $\mathbf{R}_{m \times n}$ is an upper triangular matrix with positive diagonal entries.

Based on Lemma 2.1, we are going to apply QR decomposition to spatial multiplexing MIMO systems and DSTTD systems respectively in the next two sections.

2.3.2 QR Decomposition of Channel Matrix in Spatial Multiplexing MIMO Systems

In spatial multiplexing MIMO systems, the channel matrix is defined as a standard complex Gaussian $n_R \times n_T$ matrix \mathbf{H} which has i.i.d. complex zero-mean Gaussian entries with identical variance 1. Though the QR decomposition of i.i.d. MIMO channel matrix has no special structure, there is still a lemma in random matrix theory worth mentioning.

Lemma 2.2: Let \mathbf{H} be an $m \times n$ standard complex Gaussian matrix with $n \geq m$. Denote its QR decomposition by $\mathbf{H} = \mathbf{Q}\mathbf{R}$. The upper triangular matrix \mathbf{R} is independent of \mathbf{Q} . The entries of \mathbf{R} are independent and its diagonal entries, R_{ii} for $i \in \{1, \dots, m\}$, are such that $2R_{ii}^2$ are chi-square random variables with $2(n - i + 1)$ degrees of freedom while the off-diagonal entries, R_{ij} for $i < j$, are independent zero-mean complex Gaussian with variance 1.

This lemma makes us able to develop an overall average BER criterion to construct a power allocation scheme for spatial multiplexing MIMO communication.

We will discuss it later in Chapter 3.

2.3.3 QR Decomposition of Channel Matrix in Double Space-Time Transmit Diversity Systems

First, the properties of Alamouti block are introduced. They are important in deriving the QR decomposition of DSTTD systems. We list some fundamental properties as follows:

1. The sum of two Alamouti matrices is also an Alamouti matrix.
2. The product of two Alamouti matrices is also an Alamouti matrix.
3. The inverse of an Alamouti matrix is also an Alamouti matrix.

It is easy to derive the above results and the proofs are omitted here. From the above properties, it is obvious that the Alamouti structure for block matrices is preserved if the matrix operation is performed. We arrange them and show Lemma 2.3 and Lemma 2.4 [19].

Lemma 2.3: For a square matrix $\mathbf{H}_{n \times n}$ constructed by Alamouti blocks, the inverse of $\mathbf{H}_{n \times n}$ is also constructed by Alamouti blocks. That is, it is a block matrix with Alamouti sub-blocks.

Here is a simple example to explain the above lemma. Consider a matrix $\mathbf{H}_{4 \times 4}$ with four Alamouti sub-blocks given by

$$\mathbf{H}_{4 \times 4} = \begin{bmatrix} \mathbf{H}_1 & \mathbf{H}_2 \\ \mathbf{H}_3 & \mathbf{H}_4 \end{bmatrix}, \quad (2.13)$$

where \mathbf{H}_1 , \mathbf{H}_2 , \mathbf{H}_3 , and \mathbf{H}_4 are all Alamouti block matrices, e.g.,

$$\mathbf{H}_1 = \begin{bmatrix} h_{11} & h_{12} \\ -h_{12}^* & h_{11} \end{bmatrix}, \text{ and } \mathbf{H}_2 = \begin{bmatrix} h_{13} & h_{14} \\ -h_{14}^* & h_{13} \end{bmatrix},$$

and

$$\mathbf{H}_3 = \begin{bmatrix} h_{21} & h_{22} \\ -h_{22}^* & h_{21} \end{bmatrix}, \text{ and } \mathbf{H}_4 = \begin{bmatrix} h_{23} & h_{24} \\ -h_{24}^* & h_{23} \end{bmatrix}. \quad (2.14)$$

Under some manipulations, it can be shown that all the sub-blocks in $\mathbf{H}_{4 \times 4}^{-1}$ are also Alamouti block matrices by using the fundamental properties of Alamouti structure. By this example, we can know that the inverse of channel matrix in DSTTD systems has the same structure.

Lemma 2.4: For a square matrix $\mathbf{H}_{n \times n}$ which is constructed by Alamouti sub-blocks,

assume $\mathbf{H}_{n \times n}$ is factored as $\mathbf{H}_{n \times n} = \mathbf{Q}_{n \times n} \mathbf{R}_{n \times n}$, where the columns of $\mathbf{Q}_{n \times n}$ are an orthonormal basis and $\mathbf{Q}_{n \times n}$ is a square unitary matrix. $\mathbf{R}_{n \times n}$ is an upper triangular matrix with positive diagonal entries. Then, $\mathbf{Q}_{n \times n}$ is also constructed by Alamouti sub-blocks. $\mathbf{R}_{n \times n}$ has a special structure which is a block matrix with multiples of \mathbf{I}_2 along its diagonal and with Alamouti sub-blocks in its upper triangular part. Continue with the previous example

$$\mathbf{H} = \begin{bmatrix} h_{11} & h_{12} & h_{13} & h_{14} \\ -h_{12}^* & h_{11} & -h_{14}^* & h_{13}^* \\ h_{21} & h_{22} & h_{23} & h_{24} \\ -h_{22}^* & h_{21} & -h_{24}^* & h_{23}^* \end{bmatrix}. \quad (2.15)$$

The QR decomposition of \mathbf{H} can be expressed as

$$\mathbf{Q} = \begin{bmatrix} q_{11} & q_{12} & q_{13} & q_{14} \\ * & * & * & * \\ -q_{12} & q_{11} & -q_{14} & q_{13} \\ q_{21} & q_{22} & q_{23} & q_{24} \\ * & * & * & * \\ -q_{22} & q_{21} & -q_{24} & q_{23} \end{bmatrix}, \text{ and } \mathbf{R} = \begin{bmatrix} R_{11} & 0 & R_{13} & R_{14} \\ 0 & R_{22} & -R_{14}^* & R_{13}^* \\ 0 & 0 & R_{33} & 0 \\ 0 & 0 & 0 & R_{44} \end{bmatrix}, \quad (2.16)$$

where all 2×2 sub-blocks are all Alamouti block matrices.

The proof is given in Appendix A. From the proof we can discover that the $R_{11} = R_{22}$ and $R_{33} = R_{44}$ for diagonal entries of \mathbf{R} , and they can be written in terms of determinants of channel matrix \mathbf{H} and its partitioned matrices (Alamouti sub-blocks). Finally, we can arrange the above derivations and conclude this section with the following properties:

1. The channel matrix of DSTTD systems is given by

$$\mathbf{H} = \begin{bmatrix} \mathbf{H}_1 & \mathbf{H}_2 \\ \mathbf{H}_3 & \mathbf{H}_4 \end{bmatrix} = \begin{bmatrix} h_{11} & h_{12} & h_{13} & h_{14} \\ -h_{12}^* & h_{11}^* & -h_{14} & h_{13}^* \\ h_{21} & h_{22} & h_{23} & h_{24} \\ -h_{22}^* & h_{21}^* & -h_{24} & h_{23}^* \end{bmatrix}. \quad (2.17)$$

It can be factorized as

$$\mathbf{H} = \mathbf{Q}\mathbf{R} = \begin{bmatrix} q_{11} & q_{12} & q_{13} & q_{14} \\ * & * & * & * \\ -q_{12} & q_{11} & -q_{14} & q_{13} \\ q_{21} & q_{22} & q_{23} & q_{24} \\ * & * & * & * \\ -q_{22} & q_{21} & -q_{24} & q_{23} \end{bmatrix} \begin{bmatrix} R_{11} & 0 & R_{13} & R_{14} \\ 0 & R_{22} & -R_{14}^* & R_{13}^* \\ 0 & 0 & R_{33} & 0 \\ 0 & 0 & 0 & R_{44} \end{bmatrix}. \quad (2.18)$$

2. The diagonal entries of \mathbf{R} can be expressed as

$$R_{11} = R_{22} = \sqrt{\det(\mathbf{H}_1) + \det(\mathbf{H}_3)}, \quad (2.19)$$

and

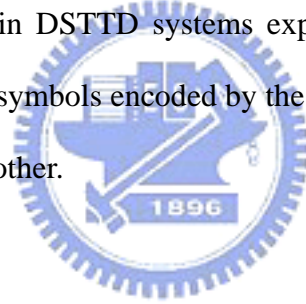
$$R_{33} = R_{44} = \sqrt{\frac{\det(\mathbf{H})}{\det(\mathbf{H}_1) + \det(\mathbf{H}_3)}}, \quad (2.20)$$

where \mathbf{H}_1 , \mathbf{H}_2 , \mathbf{H}_3 , and \mathbf{H}_4 are Alamouti sub-block in (2.17), and the determinants of them are given by

$$\det(\mathbf{H}_1) = |h_{11}|^2 + |h_{12}|^2, \quad \det(\mathbf{H}_2) = |h_{13}|^2 + |h_{14}|^2, \\ \det(\mathbf{H}_3) = |h_{21}|^2 + |h_{22}|^2, \quad \text{and} \quad \det(\mathbf{H}_4) = |h_{23}|^2 + |h_{24}|^2. \quad (2.21)$$

2.4 Model of MIMO Wireless Communication Systems with QR-Based Successive Detection

From the above discussions, in this section we will introduce the models of the two wireless communication systems. The symbol detection of QR-based receiver is based on unordered successive interference cancellation (SIC). In spatial multiplexing MIMO systems, symbol detection in one stage depends on the decisions made in the previous stages. Detection in DSTTD systems experiences the same effect, but in a group-wise manner; that is, symbols encoded by the same Alamouti space-time encoder will not interfere with each other.



2.4.1 Model of Spatial Multiplexing MIMO systems

We consider a 4×4 spatial multiplexing MIMO systems whose channel matrix is given by

$$\mathbf{H} = \begin{bmatrix} h_{11} & h_{12} & h_{13} & h_{14} \\ h_{21} & h_{22} & h_{23} & h_{24} \\ h_{31} & h_{32} & h_{33} & h_{34} \\ h_{41} & h_{42} & h_{43} & h_{44} \end{bmatrix}, \quad (2.22)$$

which can be factorized as

$$\mathbf{H} = \mathbf{QR} = \begin{bmatrix} q_{11} & q_{12} & q_{13} & q_{14} \\ q_{21} & q_{22} & q_{23} & q_{24} \\ q_{31} & q_{32} & q_{33} & q_{34} \\ q_{41} & q_{42} & q_{43} & q_{44} \end{bmatrix} \begin{bmatrix} R_{11} & R_{12} & R_{13} & R_{14} \\ 0 & R_{22} & R_{23} & R_{24} \\ 0 & 0 & R_{33} & R_{34} \\ 0 & 0 & 0 & R_{44} \end{bmatrix}. \quad (2.23)$$

Since \mathbf{R} is upper triangular, successive symbol detection through canceling the contributions of the previously detected components can be performed, as in [15], [16]. From Equations (2.2) and (2.23), the received signals are multiplied by the unitary matrix \mathbf{Q}^H to yield

$$\tilde{\mathbf{y}} = \begin{bmatrix} \tilde{y}_1 \\ \tilde{y}_2 \\ \tilde{y}_3 \\ \tilde{y}_4 \end{bmatrix} = \begin{bmatrix} R_{11} & R_{12} & R_{13} & R_{14} \\ 0 & R_{22} & R_{23} & R_{24} \\ 0 & 0 & R_{33} & R_{34} \\ 0 & 0 & 0 & R_{44} \end{bmatrix} \begin{bmatrix} x_1 \\ x_2 \\ x_3 \\ x_4 \end{bmatrix} + \begin{bmatrix} \tilde{n}_1 \\ \tilde{n}_2 \\ \tilde{n}_3 \\ \tilde{n}_4 \end{bmatrix} = \mathbf{R}\mathbf{x} + \tilde{\mathbf{n}}, \quad (2.24)$$

where $\tilde{\mathbf{y}} = \mathbf{Q}^H \mathbf{y}$ and $\tilde{\mathbf{n}} = \mathbf{Q}^H \mathbf{n}$. It is noted that $\tilde{\mathbf{n}}$ and \mathbf{n} have an identical distribution since \mathbf{Q}^H is unitary. Equation (2.24) can be expressed as follows:

$$\tilde{y}_i = R_{ii}x_i + \sum_{j=i+1}^4 R_{ij}x_j + \tilde{n}_i, \quad i = 1, 2, 3, 4. \quad (2.25)$$

Then we can get the modified received signals

$$\hat{y}_i = \tilde{y}_i - \sum_{j=i+1}^4 R_{ij}\hat{x}_j = R_{ii}x_i + \sum_{j=i+1}^4 R_{ij}(x_j - \hat{x}_j) + \tilde{n}_i, \quad i = 1, 2, 3, 4, \quad (2.26)$$

where \hat{x}_j is the symbols detected in the previous detection stages. Therefore, to detect symbol x_i , we will need to know the detected symbols \hat{x}_j ($j = i + 1, i + 2, \dots, 4$).

The detection procedure can be described by the following expressions:

$$\hat{x}_i = \text{Quant} \left[\frac{\tilde{y}_i - \sum_{j=i+1}^4 R_{ij}\hat{x}_j}{R_{ii}} \right] \text{ for } i = 1, 2, 3, 4. \quad (2.27)$$

The function $a = \text{Quant}[b]$ sets a to the element of signal constellations that is closet to b . Assuming that these decisions are correct ($x_j = \hat{x}_j$), Equation (2.26) is simplified to $\hat{y}_i = R_{ii}x_i + \tilde{n}_i$, and the decision turns out to be $\hat{x}_i = \text{Quant}[\hat{y}_i/R_{ii}]$.

This makes it convenient for us to detect the received signals.

2.4.2 Model of Double Space-Time Transmit Diversity Systems

In DSTTD systems, for its special channel matrix structure, the symbols grouped together will not affect each other. The channel matrix is given by

$$\mathbf{H} = \begin{bmatrix} h_{11} & h_{12} & h_{13} & h_{14} \\ -h_{12}^* & h_{11}^* & -h_{14}^* & h_{13}^* \\ h_{21} & h_{22} & h_{23} & h_{24} \\ -h_{22}^* & h_{21}^* & -h_{24}^* & h_{23}^* \end{bmatrix}, \quad (2.28)$$

and its QR decomposition is obtained as follows:

$$\mathbf{Q} = \begin{bmatrix} q_{11} & q_{12} & q_{13} & q_{14} \\ * & * & * & * \\ -q_{12} & q_{11} & -q_{14} & q_{13} \\ q_{21} & q_{22} & q_{23} & q_{24} \\ * & * & * & * \\ -q_{22} & q_{21} & -q_{24} & q_{23} \end{bmatrix}, \text{ and } \mathbf{R} = \begin{bmatrix} R_{11} & 0 & R_{13} & R_{14} \\ 0 & R_{11} & -R_{14}^* & R_{13}^* \\ 0 & 0 & R_{33} & 0 \\ 0 & 0 & 0 & R_{33} \end{bmatrix}. \quad (2.29)$$

Similar to the expressions in the previous section, from Equations (2.12) and (2.29), the received signals can be written as

$$\tilde{\mathbf{y}} = \begin{bmatrix} \tilde{y}_1 \\ \tilde{y}_2 \\ \tilde{y}_3 \\ \tilde{y}_4 \end{bmatrix} = \begin{bmatrix} R_{11} & 0 & R_{13} & R_{14} \\ 0 & R_{11} & -R_{14}^* & R_{13}^* \\ 0 & 0 & R_{33} & 0 \\ 0 & 0 & 0 & R_{33} \end{bmatrix} \begin{bmatrix} x_1 \\ x_2 \\ x_3 \\ x_4 \end{bmatrix} + \begin{bmatrix} \tilde{n}_1 \\ \tilde{n}_2 \\ \tilde{n}_3 \\ \tilde{n}_4 \end{bmatrix} = \mathbf{R}\mathbf{x} + \tilde{\mathbf{n}}, \quad (2.30)$$

and this equation is equivalent to

$$\begin{aligned} \tilde{y}_1 &= R_{11}x_1 + R_{13}x_3 + R_{14}x_4, \\ \tilde{y}_2 &= R_{11}x_2 - R_{14}^*x_3 + R_{13}^*x_4, \\ \tilde{y}_3 &= R_{33}x_3, \\ \tilde{y}_4 &= R_{33}x_4. \end{aligned} \quad (2.31)$$

Thus, the detection procedure can be described by the following formulas:

$$\hat{x}_4 = \text{Quant} \left[\frac{\tilde{y}_4}{R_{33}} \right], \quad \hat{x}_3 = \text{Quant} \left[\frac{\tilde{y}_3}{R_{33}} \right],$$

$$\hat{x}_2 = \text{Quant} \left[\frac{\tilde{y}_2 + R_{14}^* x_3 - R_{13}^* x_4}{R_{11}} \right],$$

$$\text{and } \hat{x}_1 = \text{Quant} \left[\frac{\tilde{y}_1 + R_{13} x_3 - R_{14} x_4}{R_{11}} \right]. \quad (2.32)$$

As we can see in Equation (2.32), x_3 and x_4 can be detected individually, and then x_1 and x_2 can be decided with the decisions made for x_3 and x_4 . The simulations are provided and compared with the MMSE detector.

2.5 Computer Simulations

In the simulation results, we first examine the performances of spatial multiplexing MIMO systems. Assume that QPSK modulation is adopted and the fading channels are flat. The channel coefficients are i.i.d. complex Gaussian random variables with zero mean and unit variance. The noise is complex zero-mean Gaussian random variable with unit variance. In Figure 2.4, the performances of spatial multiplexing MIMO systems with different numbers of transmit-receive antenna pairs and with different detection schemes are presented. As we can see in Figure 2.4, in spatial multiplexing systems with ML detection at the receiver, ML receiver is capable of extracting four-order spatial diversity because the ML detecting process outputs the most likely transmitted signal vector, so that the receiver spatial diversity can be fully obtained. The linear receivers like QR receiver and MMSE receiver can only extract one-order spatial diversity for all degrees of freedom of the transmission systems are exploited to increase the capacity. In 4×4 spatial multiplexing systems, MMSE receiver performs better than QR receiver. Further, for QR receiver, when the number of parallel channels increases, the performances degrade slightly. One reason for this is

power sharing among the transmit antennas; since the normalization keeps the total transmit energy constant, in spatial multiplexing the power per stream is reduced by a factor of n_R . Another reason is that when the number of data streams increases, in QR detection the average performances will become poorer due to cross-stage error propagation.

In DSTTD systems, the simulation results for different receivers are shown in Figure 2.5. The performances of DSTTD systems with QR receiver and MMSE receiver are quite comparable. That is, we can provide similar average BER performances with QR-based successive detection compared with the MMSE detection. Because of the transmit diversity provided by Alamouti space-time encoder, compared with the performance in 2×2 spatial multiplexing for the same transmission rate, DSTTD systems have a two-order spatial diversity which is higher than unordered spatial multiplexing schemes. With ML receiver, a four-order spatial diversity can be achieved since ML receiver is able to extract the two-order receive spatial diversity in DSTTD systems.

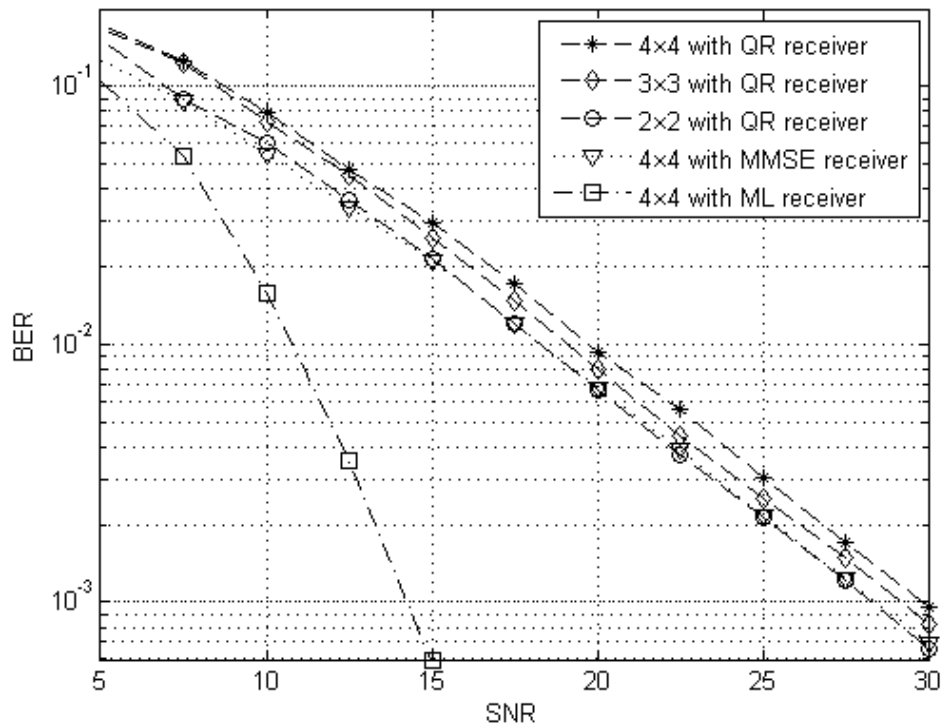


Figure 2.4: Average BER performances of spatial multiplexing MIMO systems with different receivers with QPSK modulation

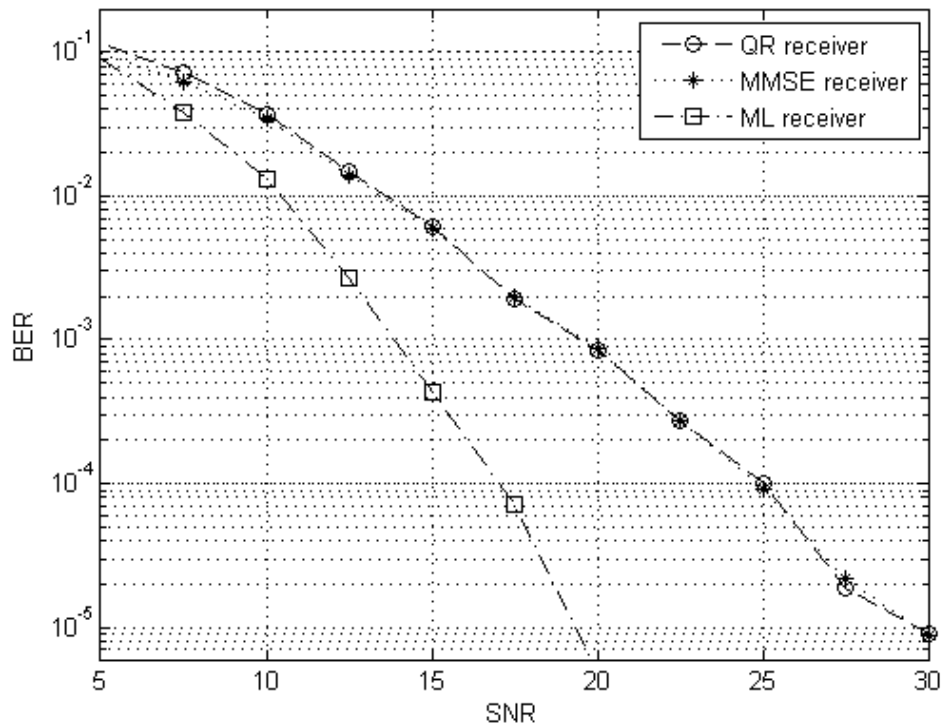


Figure 2.5: Average BER performances of DSTTD systems with different receivers with QPSK modulation

2.6 Summary

In wireless communication systems, spatial multiplexing techniques are widely used to exploit the characteristics of multipath channels and to improve the capacity of transmission without allocating extra bandwidth. On the aspect of diversity techniques, which is implemented to reduce the effects of multipath fading and to enhance the reliability of transmission without increasing the transmit power or sacrificing the bandwidth, it is popular to make use of space diversity which can be classified into two categories, transmit diversity and receive diversity. In this chapter, we focus on two high-rate wireless communication systems, simple spatial multiplexing and double space-time transmit diversity. Spatial multiplexing systems can provide a high data rate but no diversity gain can be obtained. Thus, a compromised transmission scheme, double space-time transmit diversity, is introduced. Compared to conventional SISO systems, DSTTD can provide a double rate and double diversity at the same time.

The QR decompositions of spatial multiplexing and DSTTD systems are characterized in Section 2.3. Based on the results of QR decomposition, the structures of the upper triangular matrix are shown in Equation (2.23) and (2.29). It is useful for us to detect the received signals and provide better performance. Furthermore, in DSTTD systems, we derive the diagonal entries of the upper triangular matrix and express them in terms of the determinants of the channel matrix and its partitioned matrices. Then, some performance comparisons are illustrated in Section 2.5. Since QR detector is an unordered SIC detector, its performance is slightly poorer than the performance of MMSE detector. In the next two chapters, we will exploit the precoding matrix to allocate the transmit power and reduce the average bit error rate (BER). That is, we focus on the power allocation scheme by using the statistical properties of with QR-based SIC detection in spatial multiplexing and DSTTD systems.

Chapter 3

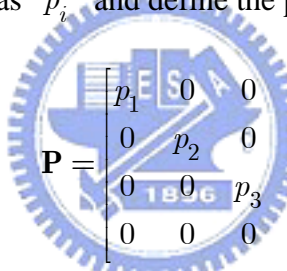
Power Allocation for Minimum BER in Spatial Multiplexing Systems

In this chapter, we will discuss the power allocation scheme with QR-based successive detection for spatial multiplexing MIMO systems over flat fading channels. Our consideration is confined to uncoded quadrature phase-shift keying (QPSK) signals and the channels are independent and identically distributed Rayleigh fading. Given that the channel state information (CSI) is perfectly available at the receiver and only signal-to-noise ratio (SNR) is known at the transmitter, we design a precoding matrix to allocate transmit power at the transmitter under average channel realizations. Furthermore, at the receiver, the received signals are detected with a QR-based successive symbol detecting scheme which is described in the previous chapter. For simplicity, the precoding matrix is restricted to be a diagonal power loading matrix so as to reduce the computational complexity. The optimization criterion is determined based on minimizing the overall average bit error rate (BER) of this transmission scheme. From the theory in [15], the design of the precoding matrix is based on the minimization of the lower bound for average BER. It can be proved that minimizing the lower bound for average BER will lead to minimizing the upper bound for the block error rate simultaneously. Following that, we exploit the power loading factors derived

from the closed-form solutions which we obtain by averaging the lower bound for BER over the channel realizations. Finally, some performance comparisons and discussions will be illustrated in the end of this chapter.

3.1 Bound for BER of QR-Based Successive Detection

Power loading schemes allocate the transmit power across symbols under the constraint of constant power per block. At the transmitter, for four symbols $x_i, i = 1, 2, 3, 4$ transmitted at the same time, we denote the transmit power allocated to the i th symbol as p_i^2 and define the power loading matrix as



$$\mathbf{P} = \begin{bmatrix} p_1 & 0 & 0 & 0 \\ 0 & p_2 & 0 & 0 \\ 0 & 0 & p_3 & 0 \\ 0 & 0 & 0 & p_4 \end{bmatrix}, \quad (3.1)$$

where $p_i > 0$ is the power loading factor, and the block transmit power constraint must be normalized as

$$\text{trace}\{\mathbf{P}^H \mathbf{P}\} = \sum_{i=1}^4 p_i^2 = 4. \quad (3.2)$$

Assuming that the channels are flat fading, we insert the power loading matrix into the system model in Equation (2.24). If the receiver replies the channel state information (CSI) to the transmitter, the transmitter can determine the power loading factors by the CSI. The block diagram with the transmit power allocation scheme is shown in Figure 3.1.

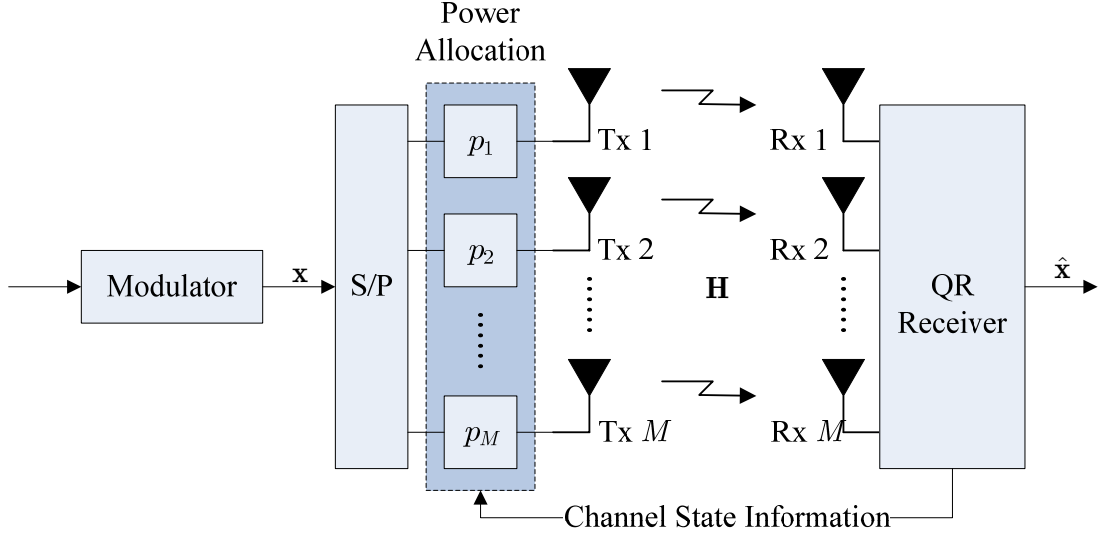


Figure 3.1: Block diagram of a 4×4 spatial multiplexing MIMO system with the QR receiver with the transmit power allocation scheme

The received signals are multiplied from the left by the unitary matrix \mathbf{Q}^H from QR decomposition, and they can be written as

$$\tilde{\mathbf{y}} = \begin{bmatrix} \tilde{y}_1 \\ \tilde{y}_2 \\ \tilde{y}_3 \\ \tilde{y}_4 \end{bmatrix} = \begin{bmatrix} R_{11} & R_{12} & R_{13} & R_{14} \\ 0 & R_{22} & R_{23} & R_{24} \\ 0 & 0 & R_{33} & R_{34} \\ 0 & 0 & 0 & R_{44} \end{bmatrix} \begin{bmatrix} p_1 & 0 & 0 & 0 \\ 0 & p_2 & 0 & 0 \\ 0 & 0 & p_3 & 0 \\ 0 & 0 & 0 & p_4 \end{bmatrix} \begin{bmatrix} x_1 \\ x_2 \\ x_3 \\ x_4 \end{bmatrix} + \begin{bmatrix} \tilde{n}_1 \\ \tilde{n}_2 \\ \tilde{n}_3 \\ \tilde{n}_4 \end{bmatrix} = \mathbf{R}\mathbf{P}\mathbf{x} + \tilde{\mathbf{n}}, \quad (3.3)$$

where $\tilde{\mathbf{y}} = \mathbf{Q}^H \mathbf{y}$ and $\tilde{\mathbf{n}} = \mathbf{Q}^H \mathbf{n}$. The i th element of modified received signals is detected as follows:

$$\hat{y}_i = \tilde{y}_i - \sum_{j=i+1}^4 R_{ij} p_j \hat{x}_j = R_{ii} p_i x_i + \sum_{j=i+1}^4 R_{ij} p_j (x_j - \hat{x}_j) + \tilde{n}_i. \quad (3.4)$$

Assume that there is no error in the previous symbol detection, and then we can obtain $\hat{y}_i = R_{ii} p_i x_i + \tilde{n}_i$. It is obvious that the i th modified received signal is determined by the i th transmitted symbol and the transformed channel noise. As long as the symbol in each stage is correctly detected and, hence, there is no layer-wise error propagation, the space-time model decouples into four independent transmission links.

The power loading factor p_i^2 represents the transmit power allocated to the i th sub-channel and R_{ii} is the i th sub-channel gain. The average energy of the symbols transmitted from each antenna is normalized to be one. Therefore, the total symbol energy E_s is equal to n_T , so that the average power of received signal at each receive antenna is also n_T . The real part and imaginary part of noise have the same variance $n_T/(2SNR)$. The average signal-to-noise ratio (SNR) is defined by $\rho \triangleq E_s/N_0$, where the total symbol energy and noise variance are defined as $E\{\mathbf{xx}^H\} = E_s \mathbf{I}_{n_T} = 4\mathbf{I}_4$ and $E\{\tilde{\mathbf{nn}}^H\} = N_0 \mathbf{I}_4$, respectively. At some ρ , the instantaneous BER under the i th sub-channel is given by

$$P_{ei} = Q(\sqrt{\rho} |p_i R_{ii}|), \quad (3.5)$$

where $Q(x) \triangleq \frac{1}{2\pi} \int_{\pi}^{\infty} e^{-y^2/2} dy$ and QPSK modulation is adopted. Thus, the average instantaneous BER of the symbol block given a fixed channel realization is expressed as

$$P_e = \frac{1}{4} \sum_{i=1}^4 P_{ei} = \frac{1}{4} \sum_{i=1}^4 Q(\sqrt{\rho} |p_i R_{ii}|). \quad (3.6)$$

It is noted that the above discussion is under the error propagation free case; that is, error propagation is not taken into account. In this case, Equation (3.6) is merely a lower bound for average BER, and we rewrite it as

$$P_{eL} = \frac{1}{4} \sum_{i=1}^4 P_{eLi} = \frac{1}{4} \sum_{i=1}^4 Q(\sqrt{\rho} |p_i R_{ii}|), \quad (3.7)$$

where the subscript L indicates the lower bound for BER. This is a lower bound with QR-based successive symbol detection without considering the error propagation. Ignoring the error propagation is a reasonable approximation at moderate-to-high

SNR regime because the error propagation is small enough to be neglected when SNR is high. If the error propagation occurs, the detection error of previous symbol decisions will affect the detection of the present symbol. This effect causes that the average BER with the error propagation is slightly higher than the average BER in the error propagation free case.

After the lower bound for average BER is presented, we will introduce the upper bound for average block error rate, which is of our major concern. First, let us define the detection error in the i th symbol x_i when there may be errors in the detection of previous symbols. We denote the received signal vector which would have been detected before x_i by $\hat{\mathbf{x}}_{ei} = [\hat{x}_{i+1}, \dots, \hat{x}_4]^T$, and the transmitted signal vector which will be detected before x_i by $\mathbf{x}_{ei} = [x_{i+1}, \dots, x_4]^T$, respectively. For the detection of the i th symbol x_i , based on Bayes' rule, we can get

$$\begin{aligned}
 P\{x_i \neq \hat{x}_i\} &= P\{x_i \neq \hat{x}_i | \mathbf{x}_{ei} = \hat{\mathbf{x}}_{ei}\} P\{\mathbf{x}_{ei} = \hat{\mathbf{x}}_{ei}\} \\
 &\quad + P\{x_i \neq \hat{x}_i | \mathbf{x}_{ei} \neq \hat{\mathbf{x}}_{ei}\} P\{\mathbf{x}_{ei} \neq \hat{\mathbf{x}}_{ei}\}.
 \end{aligned} \tag{3.8}$$

$P\{x_i \neq \hat{x}_i | \mathbf{x}_{ei} = \hat{\mathbf{x}}_{ei}\}$ is equivalent to Equation (3.5) for the error propagation free case so that Equation (3.8) can be written as

$$\begin{aligned}
 P\{x_i \neq \hat{x}_i\} &= P_{eLi} P\{\mathbf{x}_{ei} = \hat{\mathbf{x}}_{ei}\} + P\{x_i \neq \hat{x}_i | \mathbf{x}_{ei} \neq \hat{\mathbf{x}}_{ei}\} P\{\mathbf{x}_{ei} \neq \hat{\mathbf{x}}_{ei}\} \\
 &\leq P_{eLi} + P\{\mathbf{x}_{ei} \neq \hat{\mathbf{x}}_{ei}\}.
 \end{aligned} \tag{3.9}$$

In the above equation, the last inequality is due to the fact that

$P\{x_i \neq \hat{x}_i | \mathbf{x}_{ei} \neq \hat{\mathbf{x}}_{ei}\} \leq 1$ and $P\{\mathbf{x}_{ei} = \hat{\mathbf{x}}_{ei}\} \cong 1$ for high SNR. Furthermore,

$$\begin{aligned}
 P\{\mathbf{x}_{ei} \neq \hat{\mathbf{x}}_{ei}\} &= 1 - P\{\mathbf{x}_{ei} = \hat{\mathbf{x}}_{ei}\} \\
 &= 1 - P\{x_4 = \hat{x}_4\} P\{x_3 = \hat{x}_3 | x_4 = \hat{x}_4\} \cdots P\{x_{i+1} = \hat{x}_{i+1} | \mathbf{x}_{ei+1} = \hat{\mathbf{x}}_{ei+1}\}
 \end{aligned}$$

$$= 1 - \prod_{j=i+1}^4 (1 - P_{eLj}) \leq \sum_{j=i+1}^4 P_{eLj}. \quad (3.10)$$

Because $P\{x_{i+1} = \hat{x}_{i+1} | \mathbf{x}_{ei+1} = \hat{\mathbf{x}}_{ei+1}\}$ is written as $1 - P\{x_i \neq \hat{x}_i | \mathbf{x}_{ei} = \hat{\mathbf{x}}_{ei}\} = 1 - P_{eLj}$, the last equality is obtained which can be easily derived by some manipulations. Combining (3.9) and (3.10), the result is shown as

$$\begin{aligned} P\{x_i \neq \hat{x}_i\} &\leq P_{eLi} + P\{\mathbf{x}_{ei} \neq \hat{\mathbf{x}}_{ei}\} \\ &\leq P_{eLi} + \sum_{j=i+1}^4 P_{eLj} = \sum_{j=i}^4 P_{eLj} = P_{eUi}, \end{aligned} \quad (3.11)$$

where the subscript U indicates the upper bound for BER. Equation (3.11) represents the upper bound for the BER based on the consideration that there may be detection errors in the previous detected symbols. The upper bound for the average BER of four symbols is given by

$$\begin{aligned} P_{eU} &= \frac{1}{4} \sum_{i=1}^4 P_{eUi} = \frac{1}{4} \sum_{i=1}^4 \sum_{j=i}^4 P_{eLj} \\ &= \frac{1}{4} \sum_{i=1}^4 iP_{eLi} = \frac{1}{4} \sum_{i=1}^4 iQ(\sqrt{\rho} |p_i R_{ii}|). \end{aligned} \quad (3.12)$$

The last equality is achieved because the detection order follows the upper triangular structure of the matrix. In view of the block error rate, let $i = 0$ in (3.11), we have

$$P\{\mathbf{x} \neq \hat{\mathbf{x}}\} = P\{\mathbf{x}_{e0} \neq \hat{\mathbf{x}}_{e0}\} \leq \sum_{i=1}^4 P_{eLi} = 4P_{eL}. \quad (3.13)$$

It is obvious that the block error rate $P\{\mathbf{x} \neq \hat{\mathbf{x}}\}$ is upper bounded by four times the lower bound for the average BER P_{eL} . This is an important result for us to determine the power allocation factors. If a power allocation matrix is designed to minimize the lower bound for the average BER, it simultaneously minimizes the upper bound for the block error rate as well. From the above derivations, the minimization of lower bound for the average BER is reasonable because we can minimize the upper bound for the block error rate at the same time. It implies that the decision performance can be

potentially improved even in the presence of cross-layer error propagation. In the next section, we will propose a power allocation scheme to minimize the overall average BER over average channel realizations with this lower bound for BER.

3.2 Optimal Power Allocation for Minimum Upper Bound of Overall Average BER

In the previous section, it has been shown that, given a fixed channel realization, the design criterion for power allocation to minimize the average BER can be modified to minimize the lower bound for average BER

$$P_{eL|\mathbf{H}} = \frac{1}{4} \sum_{i=1}^4 Q(\sqrt{\rho} |p_i R_{ii}|), \quad (3.14)$$

instead of minimization of the upper bound for the block error rate. Now we would like to consider the channel probability density function (pdf) in deriving the error probability. We consider the general case assuming $M = n_T = n_R$; i.e., there are M parallel transmission links in the spatial multiplexing MIMO systems, and the lower bound in (3.14) is expressed as

$$P_{eL|\mathbf{H}} = \frac{1}{M} \sum_{i=1}^M Q(\sqrt{\rho} |p_i R_{ii}|). \quad (3.15)$$

First of all, we have to determine the distribution of $|R_{ii}|$. From Lemma 2.2, we have known that $2R_{ii}^2$ is a chi-square random variable with $2(M - i + 1)$ degrees of freedom; that is,

$$p(2|R_{ii}|^2) = \frac{(2|R_{ii}|^2)^{M-i} e^{-|R_{ii}|^2}}{2^{M-i+1} \Gamma(M - i + 1)}. \quad (3.16)$$

Let $r_i = |R_{ii}|$ for convenience, and with some variable transformations, it is shown [20] that the pdf of $|R_{ii}|$ can be expressed as

$$p(r_i) = \frac{2r_i^{2(M-i)+1} e^{-r_i^2}}{(M-i)!}. \quad (3.17)$$

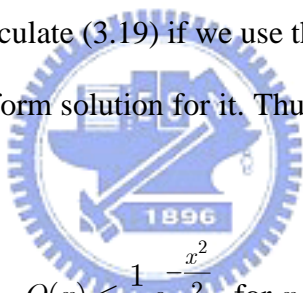
Hence, the lower bound for the overall detection error rate of x_i is given by

$$\bar{P}_{eLi} = \int_0^\infty P_{eLi|\mathbf{H}} p(r_i) dr_i = \int_0^\infty Q(\sqrt{\rho} |p_i| r_i) \frac{2r_i^{2(M-i)+1} e^{-r_i^2}}{(M-i)!} dr_i. \quad (3.18)$$

The lower bound for the overall average BER for the data block is given by

$$\bar{P}_{eL} = \frac{1}{M} \sum_{i=1}^M \bar{P}_{eLi} = \frac{1}{M} \sum_{i=1}^M \int_0^\infty Q(\sqrt{\rho} |p_i| r_i) \frac{2r_i^{2(M-i)+1} e^{-r_i^2}}{(M-i)!} dr_i. \quad (3.19)$$

It is very difficult to calculate (3.19) if we use the definition of Q-function directly, and there will be no closed-form solution for it. Thus, we substitute Q-function with its Chernoff bound



$$Q(x) \leq \frac{1}{2} e^{-\frac{x^2}{2}}, \text{ for } x \geq 0, \quad (3.20)$$

and obtain an upper bound of (3.19) given by

$$\bar{P}_{eL} \leq \frac{1}{M} \sum_{i=1}^M \int_0^\infty \left(\frac{1}{2} e^{-\frac{1}{2} \rho |p_i|^2 r_i^2} \right) \frac{2r_i^{2(M-i)+1} e^{-r_i^2}}{(M-i)!} dr_i. \quad (3.21)$$

After some rearrangements, we can rewrite this bound as

$$\bar{P}_{eL} \leq \frac{1}{M} \sum_{i=1}^M \frac{1}{(M-i)!} \int_0^\infty r_i^{2(M-i)+1} e^{-r_i^2(1+\frac{1}{2}\rho|p_i|^2)} dr_i. \quad (3.22)$$

In order to calculate the above integrand, we use a known integration formula shown as follows:

$$\int_0^\infty x^{2n+1} e^{-px^2} dx = \frac{n!}{2p^{n+1}} \text{ for } p > 0 \text{ and } n = 0, 1, 2, \dots \quad (3.23)$$

In the above equation, let $x = r_i$, $p = 1 + \rho |p_i|^2 / 2$, and $n = M - i$, the upper bound in Equation (3.22) can be expressed as

$$\begin{aligned}
\bar{P}_{eL} &\leq \frac{1}{M} \sum_{i=1}^M \frac{1}{(M-i)!} \int_0^{\infty} r_i^{2(M-i)+1} e^{-r_i^2(1+\frac{1}{2}\rho|p_i|^2)} dr_i \\
&= \frac{1}{M} \sum_{i=1}^M \frac{1}{(M-i)!} \cdot \frac{(M-i)!}{2(1+\frac{1}{2}\rho|p_i|^2)^{M-i+1}} \\
&= \frac{1}{2M} \sum_{i=1}^M (1+\frac{1}{2}\rho|p_i|^2)^{-(M-i+1)},
\end{aligned} \tag{3.24}$$

where M is the number of transmission links. Based on the above result, we can find a set of p_i to minimize this upper bound, and, hence, minimize \bar{P}_{eL} .

To find the set of p_i to minimize the upper bound with the power constraint on the elements p_i , we can formulate an optimization problem as follows:

$$\begin{aligned}
\min_{p_i} & \frac{1}{2M} \sum_{i=1}^M (1+\frac{1}{2}\rho|p_i|^2)^{-(M-i+1)} \\
\text{s.t.} & \sum_{i=1}^M |p_i|^2 = M,
\end{aligned} \tag{3.25}$$

which can be solved by the Lagrange multipliers technique. First, we define

$$F \triangleq \frac{1}{2M} \sum_{i=1}^M (1+\frac{1}{2}\rho|p_i|^2)^{-(M-i+1)} + \lambda(\sum_{i=1}^M |p_i|^2 - M). \tag{3.26}$$

By Lagrange multipliers, the optimization problem is transformed into

$$\nabla F = 0. \tag{3.27}$$

Assuming $a_i = |p_i|^2$, we can get

$$\begin{aligned}
\frac{\partial F}{\partial a_i} &= -\frac{1}{2M} \cdot \frac{\rho}{2} (M-i+1) \left(1 + \frac{1}{2} \rho a_i\right)^{-(M-i+2)} + \lambda = 0 \\
\Rightarrow \left(1 + \frac{1}{2} \rho a_i\right)^{-(M-i+2)} &= \lambda \left/ \left(\frac{1}{2M} \cdot \frac{\rho}{2} (M-i+1) \right) \right. \\
\Rightarrow \left(1 + \frac{1}{2} \rho a_i\right)^{M-i+2} &= \frac{\rho(M-i+1)}{4M\lambda} \\
\Rightarrow a_i &= \frac{2}{\rho} \left[\left(\frac{\rho(M-i+1)}{4M\lambda} \right)^{\frac{1}{M-i+2}} - 1 \right].
\end{aligned} \tag{3.28}$$

We substitute a_i for $|p_i|^2$ in the power constraint $\sum_{i=1}^M |p_i|^2 = M$, and we can obtain the constraint with an unknown variable λ as follows:

$$\begin{aligned}
\sum_{i=1}^M \frac{2}{\rho} \left[\left(\frac{\rho(M-i+1)}{4M\lambda} \right)^{\frac{1}{M-i+2}} - 1 \right] &= M \\
\Rightarrow \sum_{i=1}^M \left(\frac{\rho(M-i+1)}{4M\lambda} \right)^{\frac{1}{M-i+2}} - 1 &= \frac{\rho M}{2} \\
\Rightarrow \sum_{i=1}^M \left(\frac{\rho(M-i+1)}{4M\lambda} \right)^{\frac{1}{M-i+2}} &= \frac{\rho M}{2} + M.
\end{aligned} \tag{3.29}$$

From the above derivations, a method of determining the power loading factors by minimizing the average BER upper bound in (3.24) subject to the power normalization constraint is proposed. We propose to determine the power loading factors by minimizing the upper bound of the error probability averaged with respect to the channel distribution. As long as λ is determined, each power loading factor p_i will be determined as well. However, it is very difficult to calculate an explicit solution for λ , though it is possible to find a suitable solution λ for a set of p_i . Since we have already derived a closed-form expression for the upper bound of \bar{P}_{eL} in (3.24) as

$$B_{U, \bar{P}_{eL}} = \frac{1}{2M} \sum_{i=1}^M \left(1 + \frac{1}{2} \rho |p_i|^2\right)^{-(M-i+1)}, \tag{3.30}$$

the optimization problem can be solved via numerical search instead (e.g. by using *fmincon* function in Optimization Toolbox in MATLAB). Some average BER performances are shown in the next section followed by a brief summary.

3.3 Computer Simulations

We use *fmincon* function in MATLAB [10] which employs sequential quadratic programming to find the optimal power loading factors that minimize the upper bound for the overall average BER. We, for example, consider a 4×4 spatial multiplexing MIMO wireless communication systems with QPSK modulation scheme. First, we compare the evaluations of the upper bound for the lower bound for overall average BER without and with the transmit power allocation scheme proposed. The evaluation results are shown in Figure 3.2. It can be seen that in theory, the lower bound for the overall average BER has a 5-dB improvement at the high SNR regime when the power loading scheme is applied. However, this is just the theoretical result, and the computer simulations are shown in Figure 3.3. In Figure 3.3, it can be seen that at medium-high SNR the BER performance with power loading is improved by about 2 dB compared with that without power loading. The performance of QR receiver with power loading closely approaches that of ZF-VBLAST receiver, whose detecting procedure is more complex. In Figure 3.4, the performances with different modulation orders for QR receiver with and without power loading are shown. Since in the above derivation, for different modulation orders, the design criterion can be modified with different BER performance bounds [21], it can be seen that the performances are improved as long as the power loading factors for different modulation orders are determined. However, for higher modulation orders, the improvements in BER performances are less significant;

for example, the improvement with 16QAM becomes around 1 dB. This is because that the number of nearest neighbors in the modulation constellation increases when the constellation size gets larger.

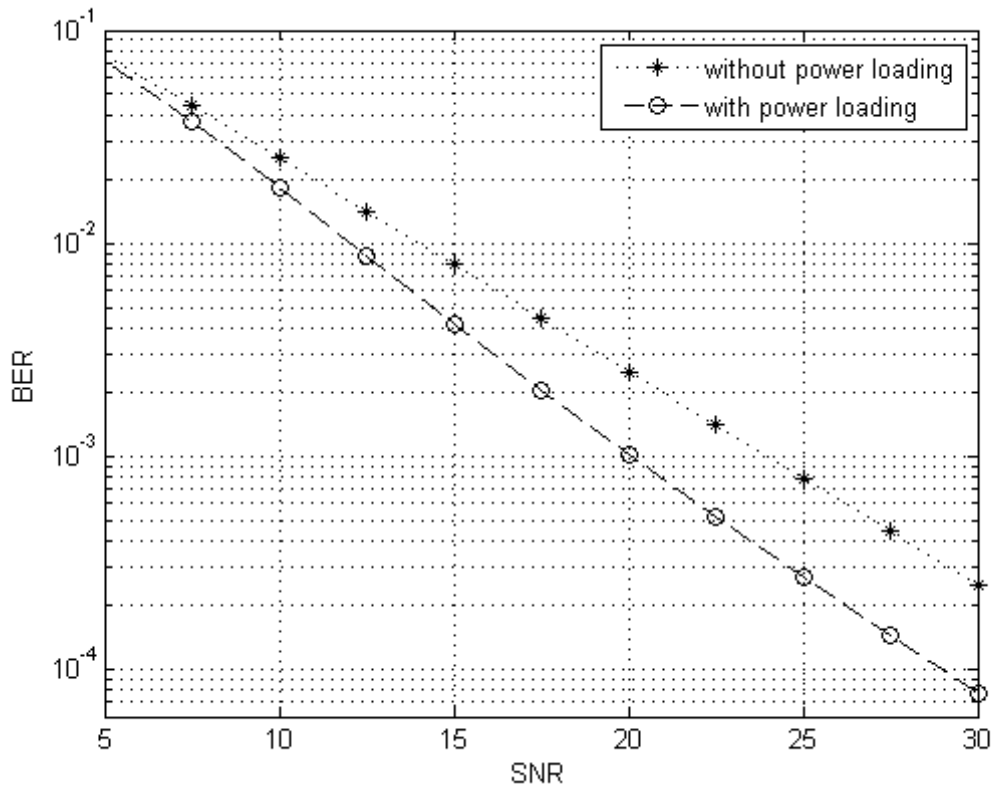


Figure 3.2: Evaluations of upper bounds for the lower bound of overall average BER in 4×4 spatial multiplexing systems with the QR receiver with QPSK modulation

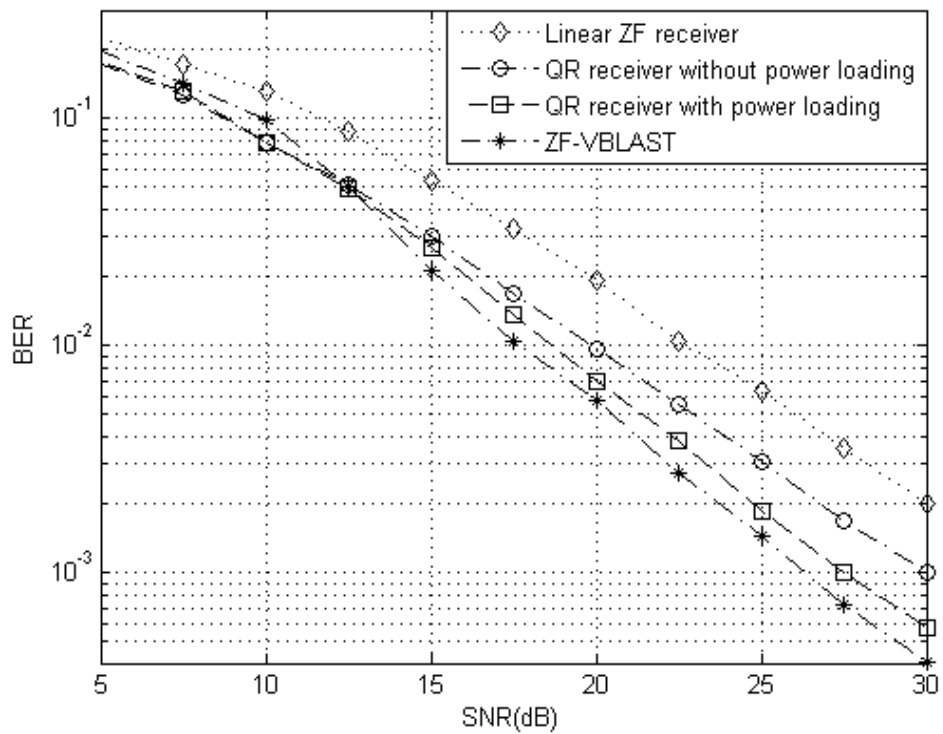


Figure 3.3: Average BER performances of 4×4 spatial multiplexing systems with different receivers with QPSK modulation

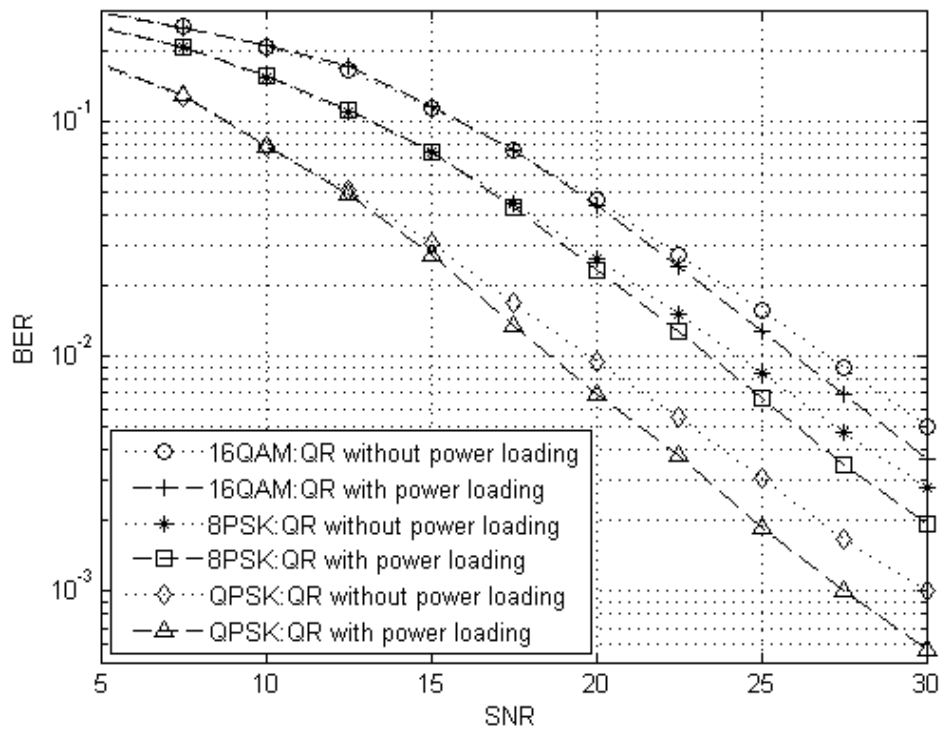


Figure 3.4: Average BER performances of 4×4 spatial multiplexing systems with the QR receivers with different modulation orders

3.4 Summary

In Section 3.1, a BER performance analysis based on spatial multiplexing MIMO systems with QR-based successive symbol detection is introduced. For simplicity, we consider the error propagation free case and derive the lower bound for the average BER. Following that, it is proved that minimization of this lower bound minimizes the upper bound for the block error rate, and thus essentially minimizes the average BER. Nevertheless, in the above discussion, we focus on the design criterion under a fixed channel realization. With the probability distribution based on QR decomposition over channel realizations shown in Chapter 2, we can obtain the lower bound for the overall average BER. An upper bound for the expression of this lower bound is obtained by using Chernoff bound of Q-function, and then this upper bound can be expressed in closed form. In the proposed power allocation scheme, the transmit power is allocated based on the power loading factors which minimize this closed-form expression. Due to that the power loading factors are derived from the performance bound over random channel realizations, and there is no need to calculate them for each given channel realization, the computational complexity is quite low. Furthermore, from Equation (3.30), the bound is only affected by the number of transmission links M and SNR ρ . This simplicity makes it possible to construct a precoding table based on different SNR for a given spatial multiplexing MIMO system. In simulations, the results show that this power allocation scheme can enhance the performances of spatial multiplexing MIMO systems by 1-2 dB, and it can be adapted according to different modulation orders.

Chapter 4

Power Allocation for Minimum BER in Double Space-Time Transmit Diversity Systems

In the previous chapter, the performance analysis of spatial multiplexing MIMO systems with the QR-based successive detection is given and a transmit power allocation scheme based on it is proposed. Now, we focus on the double space-time transmit diversity (DSTTD) systems which combines the advantages of higher data rates and transmit diversity. Since DSTTD systems can be considered as involving two parallel links in wireless transmission, with each link being space-time encoded by an Alamouti encoder, a DSTTD system can be analyzed as a 2×2 spatial multiplexing MIMO system with transmit diversity provided at the transmitter. In Chapter 2, the R matrix of QR decomposition in DSTTD systems is shown to have a special structure; we will examine the distribution of each diagonal entry of the R matrix in this chapter. Although the exact probability density functions (pdf) of the diagonal entries of the R matrix may not be easily determined, they can still be estimated and approximated reasonably to be chi-square distributed. Therefore, this result makes it possible for us to derive the design criterion of the power allocation scheme for DSTTD systems in a way similar to the derivations in Chapter 2.

4.1 Distribution of Diagonal Elements of \mathbf{R} Matrix in QR Decomposition

The QR decomposition of channel matrix in DSTTD systems is shown below:

$$\mathbf{H} = \mathbf{QR} = \begin{bmatrix} q_{11} & q_{12} & q_{13} & q_{14} \\ -q_{12}^* & q_{11}^* & -q_{14}^* & q_{13}^* \\ q_{21} & q_{22} & q_{23} & q_{24} \\ -q_{22}^* & q_{21}^* & -q_{24}^* & q_{23}^* \end{bmatrix} \begin{bmatrix} R_{11} & 0 & R_{13} & R_{14} \\ 0 & R_{22} & -R_{14}^* & R_{13}^* \\ 0 & 0 & R_{33} & 0 \\ 0 & 0 & 0 & R_{44} \end{bmatrix}. \quad (4.1)$$

Since $R_{11} = R_{22}$ and $R_{33} = R_{44}$, only the pdfs of R_{11} and R_{33} need to be determined. First, we examine the value of R_{11} . From Appendix A, it can be shown that

$$R_{11} = \sqrt{\det(\mathbf{H}_1) + \det(\mathbf{H}_3)}. \quad (4.2)$$

Because \mathbf{H}_1 and \mathbf{H}_3 are Alamouti block matrices, their determinants are given by

$$\begin{aligned} \det(\mathbf{H}_1) &= |h_{11}|^2 + |h_{12}|^2, \text{ and} \\ \det(\mathbf{H}_3) &= |h_{21}|^2 + |h_{22}|^2. \end{aligned} \quad (4.3)$$

Thus, R_{11} can be expressed as

$$\begin{aligned} R_{11} &= \sqrt{\det(\mathbf{H}_1) + \det(\mathbf{H}_3)} \\ &= \sqrt{|h_{11}|^2 + |h_{12}|^2 + |h_{21}|^2 + |h_{22}|^2}. \end{aligned} \quad (4.4)$$

In the model of DSTTD systems, we assume that h_{ij} is a complex zero-mean Gaussian random variable and the variances of the real part and the imaginary part of it are 0.5. It can be readily proved that $2|h_{ij}|^2$ has a chi-square distribution with two degrees of freedom. As a result, we can write Equation (4.4) as

$$\begin{aligned} R_{11}^2 &= |h_{11}|^2 + |h_{12}|^2 + |h_{21}|^2 + |h_{22}|^2 \\ \Rightarrow 2R_{11}^2 &= 2|h_{11}|^2 + 2|h_{12}|^2 + 2|h_{21}|^2 + 2|h_{22}|^2. \end{aligned} \quad (4.5)$$

According to the fact that the sum of chi-square random variables is still a chi-square random variable, and its degrees of freedom is the sum of the degrees of freedom of the summands, $2|R_{11}|^2$ is also a chi-square random variable with eight degrees of freedom. Compared with the result of spatial multiplexing systems, the pdf of $2|R_{11}|^2$ is expressed as

$$p(2|R_{11}|^2) = \frac{(2|R_{11}|^2)^{4-1} e^{-|R_{11}|^2}}{2^4 \Gamma(4)}, \quad (4.6)$$

which is identical to the pdf of $2|R_{11}|^2$ in spatial multiplexing systems. Therefore, let $r_1 = |R_{11}|$, and the pdf of $|R_{11}|$ is given by

$$p(r_1) = \frac{2r_1^{2(4-1)+1} e^{-r_1^2}}{(4-1)!}. \quad (4.7)$$

Afterwards, we examine the distribution of $|R_{33}|$. From Appendix A, it is given that

$$R_{33} = \sqrt{\frac{\det(\mathbf{H})}{\det(\mathbf{H}_1) + \det(\mathbf{H}_3)}}. \quad (4.8)$$

For the convenience for the derivations below, we denote $d_i = \det(\mathbf{H}_i)$, and thus we rewrite Equation (4.8) as

$$R_{33} = \sqrt{\frac{\det(\mathbf{H})}{d_1 + d_3}}. \quad (4.9)$$

In order to express $\det(\mathbf{H})$ in terms of d_1 , d_2 , d_3 , and d_4 , we introduce the theorem of the determinant of partitioned matrices:

Theorem 4.1: Let \mathbf{M} be a square matrix partitioned as

$$\mathbf{M} = \begin{bmatrix} \mathbf{A} & \mathbf{B} \\ \mathbf{C} & \mathbf{D} \end{bmatrix}. \quad (4.10)$$

Then

$$\det(\mathbf{M}) = \det(\mathbf{A}) \det(\mathbf{D} - \mathbf{C}\mathbf{A}^{-1}\mathbf{B}), \text{ if } \mathbf{A} \text{ is invertible.} \quad (4.11)$$

It is very easy to prove this theorem. When \mathbf{A}^{-1} exists, it is easy to verify that

$$\begin{bmatrix} \mathbf{I}_m & \mathbf{0}_{m,n} \\ -\mathbf{C}\mathbf{A}^{-1} & \mathbf{I}_n \end{bmatrix} \begin{bmatrix} \mathbf{A} & \mathbf{B} \\ \mathbf{C} & \mathbf{D} \end{bmatrix} = \begin{bmatrix} \mathbf{A} & \mathbf{B} \\ \mathbf{0}_{n,m} & \mathbf{D} - \mathbf{C}\mathbf{A}^{-1}\mathbf{B} \end{bmatrix}. \quad (4.12)$$

By taking determinants for both sides, we have

$$\begin{aligned} \det(\mathbf{M}) &= \begin{vmatrix} \mathbf{A} & \mathbf{B} \\ \mathbf{0}_{n,m} & \mathbf{D} - \mathbf{C}\mathbf{A}^{-1}\mathbf{B} \end{vmatrix} \\ &= \det(\mathbf{A}) \det(\mathbf{D} - \mathbf{C}\mathbf{A}^{-1}\mathbf{B}). \end{aligned} \quad (4.13)$$

Applying Theorem 4.1 in (4.9), we can obtain

$$\begin{aligned} R_{33} &= \sqrt{\frac{\det(\mathbf{H}_1) \det(\mathbf{H}_4 - \mathbf{H}_3\mathbf{H}_1^{-1}\mathbf{H}_2)}{d_1 + d_3}} \\ &= \frac{\sqrt{d_1 \det(\mathbf{H}_4 - \mathbf{H}_3\mathbf{H}_1^{-1}\mathbf{H}_2)}}{\sqrt{d_1 + d_3}}. \end{aligned} \quad (4.14)$$

In the above equation, after some calculations, it can be shown that

$$\begin{aligned} \det(\mathbf{H}_4 - \mathbf{H}_3\mathbf{H}_1^{-1}\mathbf{H}_2) &= \det(\mathbf{H}_4) + \frac{\det(\mathbf{H}_3) \det(\mathbf{H}_2) - 2C}{\det(\mathbf{H}_1)} \\ &= d_4 + \frac{d_3 d_2 - 2C}{d_1}, \end{aligned} \quad (4.15)$$

where

$$\begin{aligned} C &= \text{Re}\{h_{23}(h_{21}^* h_{11} h_{13}^* + h_{21}^* h_{14} h_{12}^* + h_{22}^* h_{12} h_{13}^* - h_{22}^* h_{14} h_{11}^*) \\ &\quad + h_{24}(h_{21}^* h_{14}^* h_{11} + h_{22}^* h_{11}^* h_{13} + h_{22}^* h_{14}^* h_{12} - h_{21}^* h_{12}^* h_{13})\}. \end{aligned}$$

Consequently, Equation (4.14) can be expressed as

$$R_{33} = \sqrt{\frac{d_1 d_4 + d_3 d_2 - 2C}{d_1 + d_3}}. \quad (4.16)$$

To keep the consistency, we want to determine the distribution of $2|R_{33}|^2$, which is written as follows:

$$2|R_{33}|^2 = 2 \cdot \frac{d_1 d_4 + d_2 d_3 - 2C}{d_1 + d_3}. \quad (4.17)$$

Although, based on the derivations for $|R_{11}|$, it can be shown that $2d_i$, $i = 1, 2, 3, 4$ are chi-square-distributed with four degrees of freedom, there is no particular distribution suitable for this random variable. However, it can be observed that $2|R_{33}|^2$ consists of four i.i.d. chi-square random variables and a zero-mean variable with an unknown distribution. Based on this observation, we use the gamma distribution to approximate $2|R_{33}|^2$ because the chi-square distribution can be considered as a special case of the gamma distribution. The pdf of gamma distribution $Gamma(k, \theta)$ is given by

$$p(x | k, \theta) = \frac{x^{k-1} e^{-\frac{x}{\theta}}}{\theta^k \Gamma(k)}, \quad (4.18)$$

where k and θ are the parameters which affect the shape and the scale of gamma distribution respectively. Here, we use *dfittool* in MATLAB to adjust the parameters of the gamma pdf and find the fit pdf which approaches the distribution of $2|R_{33}|^2$ closely. In Figure 4.1, when $k = 2$ and $\theta = 2$ in (4.18), we can see that the curve of the gamma pdf is quite close to the sampled data of $2|R_{33}|^2$.

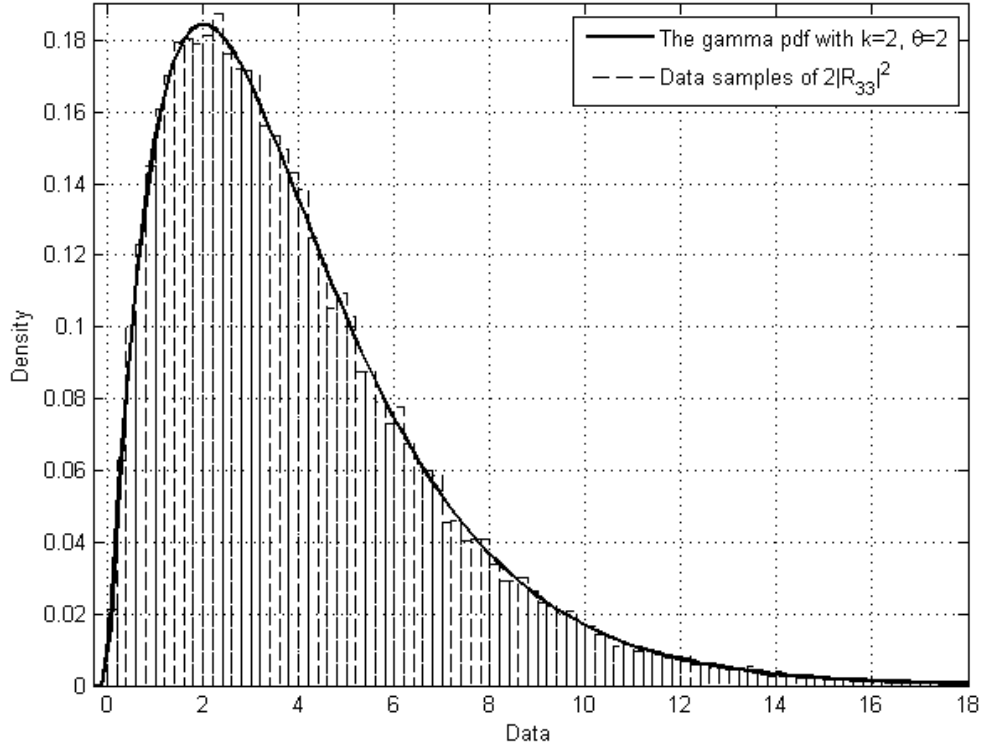
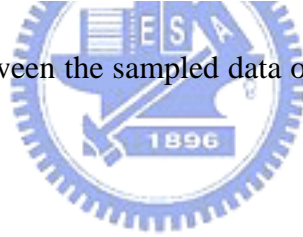


Figure 4.1: Comparison between the sampled data of $2|R_{33}|^2$ and the gamma pdf with $k = 2$ and $\theta = 2$



Therefore, this approximation makes it reasonable and accurate to assume that $2|R_{33}|^2$ is a random variable following the gamma distribution with $k = 2$ and $\theta = 2$, and its pdf is given by

$$p(2|R_{33}|^2) = \frac{2|R_{33}|^2 e^{-|R_{33}|^2}}{2^2\Gamma(2)} = \frac{(2|R_{33}|^2)^{2-1} e^{-|R_{33}|^2}}{2^2\Gamma(2)}. \quad (4.19)$$

It is obvious that (4.19) is the pdf of a chi-square distribution with four degrees of freedom as well. With some derivations similar to Chapter 3, denoting $r_3 = |R_{33}|$, the estimated pdf of $|R_{33}|$ can be expressed as

$$p(r_3) = \frac{2r_3^{2(2-1)+1} e^{-r_3^2}}{(2-1)!}. \quad (4.20)$$

Thus, since the pdfs of $|R_{11}|$ and $|R_{33}|$ are obtained, the bound for the overall average BER can be calculated.

4.2 Optimal Power Allocation for Minimum Upper Bound of Overall Average BER

Consider a 4×2 DSTTD system with QR successive detection at the receiver. Assume that the channels are flat fading, and the noises are complex Gaussian random variables with zero mean and unit variance. At the transmitter, the transmit power, which is determined by the CSI, is allocated to each transmit symbols before being encoded by the Alamouti space-time encoders. The received signals are detected by the QR receiver, and thus the modified received symbol vectors can be written as

$$\underbrace{\begin{bmatrix} \tilde{y}_1 \\ \tilde{y}_2 \\ \tilde{y}_3 \\ \tilde{y}_4 \end{bmatrix}}_{\tilde{\mathbf{y}}} = \underbrace{\begin{bmatrix} R_{11} & 0 & R_{13} & R_{14} \\ 0 & R_{11} & -R_{14}^* & R_{13}^* \\ 0 & 0 & R_{33} & 0 \\ 0 & 0 & 0 & R_{33} \end{bmatrix}}_{\mathbf{R}} \underbrace{\begin{bmatrix} p_1 & 0 & 0 & 0 \\ 0 & p_2 & 0 & 0 \\ 0 & 0 & p_3 & 0 \\ 0 & 0 & 0 & p_4 \end{bmatrix}}_{\mathbf{P}} \underbrace{\begin{bmatrix} x_1 \\ x_2 \\ x_3 \\ x_4 \end{bmatrix}}_{\mathbf{x}} + \underbrace{\begin{bmatrix} \tilde{n}_1 \\ \tilde{n}_2 \\ \tilde{n}_3 \\ \tilde{n}_4 \end{bmatrix}}_{\tilde{\mathbf{n}}} = \mathbf{R}\mathbf{P}\mathbf{x} + \tilde{\mathbf{n}}. \quad (4.21)$$

The block diagram of a DSTTD system with the QR receiver with the transmit power allocation scheme is shown in Figure 4.2.

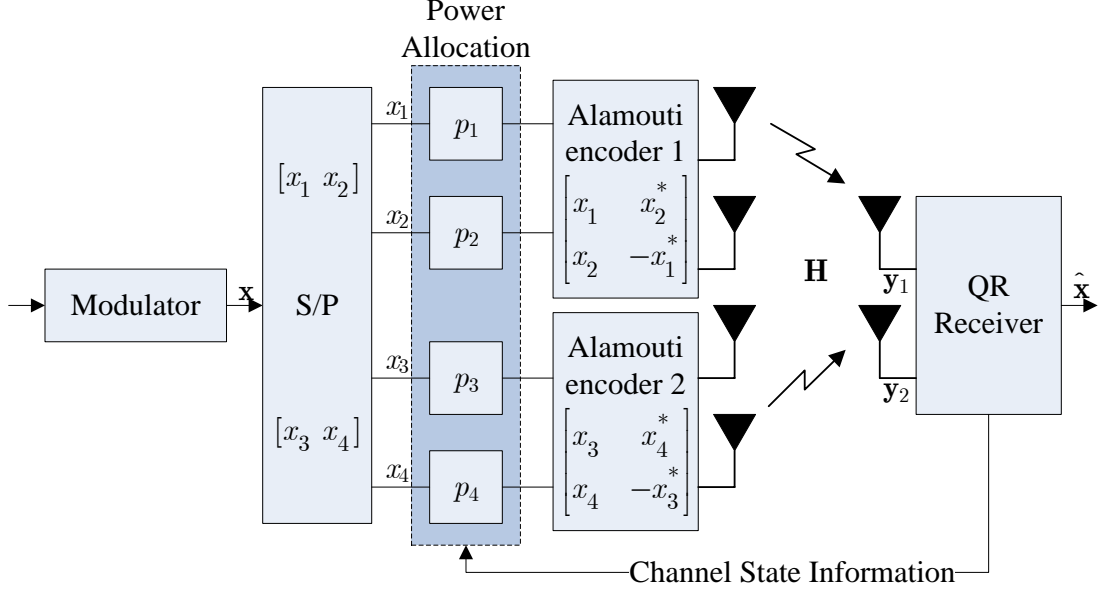


Figure 4.2: Block diagram of a DSTTD system with the QR receiver with transmit power allocation scheme

With the pdfs of $|R_{11}|$ and $|R_{33}|$, the lower bound for average BER we derived in Section 3.2 can be adopted as the criterion for us to design the power allocation scheme for DSTTD systems. Assuming QPSK modulation is adopted, the lower bound for average BER in DSTTD systems is given by

$$P_{eL|\mathbf{H}} = \frac{1}{4} \sum_{i=1}^4 Q(\sqrt{\rho} |p_i R_{ii}|). \quad (4.22)$$

According to the results of QR decomposition in DSTTD systems, it is known that

$R_{11} = R_{22}$ and $R_{33} = R_{44}$. Further, the pdf of $R_{11} = R_{22}$ is given by

$$p(r_1) = P(|R_{11}|) = P(|R_{22}|) = \frac{2r_1^{2(4-1)+1} e^{-r_1^2}}{(4-1)!}, \quad (4.23)$$

and the estimated pdf of $R_{33} = R_{44}$ is given by

$$p(r_3) = P(|R_{33}|) = P(|R_{44}|) = \frac{2r_3^{2(2-1)+1} e^{-r_3^2}}{(2-1)!}. \quad (4.24)$$

Therefore, the lower bound for average BER can be written as

$$\begin{aligned}
\bar{P}_{eL} &= \frac{1}{4} \sum_{i=1}^4 \bar{P}_{eLi} \\
&= \frac{1}{4} \left[\sum_{i=1}^2 \int_0^{\infty} Q(\sqrt{\rho} |p_i| r_1) \frac{2r_1^{2(4-1)+1} e^{-r_1^2}}{(4-1)!} dr_1 \right. \\
&\quad \left. + \sum_{i=3}^4 \int_0^{\infty} Q(\sqrt{\rho} |p_i| r_3) \frac{2r_3^{2(2-1)+1} e^{-r_3^2}}{(2-1)!} dr_3 \right].
\end{aligned} \tag{4.25}$$

With the Chernoff bound of Q-function (3.20), we can obtain an upper bound for the above equation which is written as

$$\begin{aligned}
\bar{P}_{eL} &\leq \frac{1}{4} \left[\sum_{i=1}^2 \int_0^{\infty} \frac{1}{2} e^{-\frac{1}{2}\rho |p_i|^2 r_1^2} \frac{2r_1^{2(4-1)+1} e^{-r_1^2}}{(4-1)!} dr_1 \right. \\
&\quad \left. + \sum_{i=3}^4 \int_0^{\infty} \frac{1}{2} e^{-\frac{1}{2}\rho |p_i|^2 r_3^2} \frac{2r_3^{2(2-1)+1} e^{-r_3^2}}{(2-1)!} dr_3 \right] \\
&= \frac{1}{4} \left[\sum_{i=1}^2 \frac{1}{(4-1)!} \int_0^{\infty} r_1^{2(4-1)+1} e^{r_1^2(1+\frac{1}{2}\rho |p_i|^2)} dr_1 \right. \\
&\quad \left. + \sum_{i=3}^4 \frac{1}{(2-1)!} \int_0^{\infty} r_3^{2(2-1)+1} e^{r_3^2(1+\frac{1}{2}\rho |p_i|^2)} dr_3 \right].
\end{aligned} \tag{4.26}$$

Using the integration formula in (3.23), we can calculate the integrands in Equation (4.26) as follows:

$$\begin{aligned}
\bar{P}_{eL} &\leq \frac{1}{4} \left[\sum_{i=1}^2 \frac{1}{(4-1)!} \int_0^{\infty} r_1^{2(4-1)+1} e^{r_1^2(1+\frac{1}{2}\rho |p_i|^2)} dr_1 \right. \\
&\quad \left. + \sum_{i=3}^4 \frac{1}{(2-1)!} \int_0^{\infty} r_3^{2(2-1)+1} e^{r_3^2(1+\frac{1}{2}\rho |p_i|^2)} dr_3 \right] \\
&= \frac{1}{4} \left[\sum_{i=1}^2 \frac{1}{(4-1)!} \cdot \frac{(4-1)!}{2(1+\frac{1}{2}\rho |p_i|^2)^4} + \sum_{i=3}^4 \frac{1}{(2-1)!} \cdot \frac{(2-1)!}{2(1+\frac{1}{2}\rho |p_i|^2)^2} \right] \\
&= \frac{1}{8} \left[\sum_{i=1}^2 (1+\frac{1}{2}\rho |p_i|^2)^{-4} + \sum_{i=3}^4 (1+\frac{1}{2}\rho |p_i|^2)^{-2} \right].
\end{aligned} \tag{4.27}$$

Equation (4.27) is similar to the results in Chapter 3, but, however, the summands in

(4.27) are arranged into two groups. The reason for this is that the transmit symbols are divided into two groups, and the two symbols in each group are coupled by the Alamouti encoders, respectively.

Based on the result, the optimization problem to find the set of p_i can be formulated as follows:

$$\begin{aligned} \min_{p_i} \quad & \frac{1}{8} \left(\sum_{i=1}^2 \left(1 + \frac{1}{2} \rho |p_i|^2\right)^{-4} + \sum_{i=3}^4 \left(1 + \frac{1}{2} \rho |p_i|^2\right)^{-2} \right) \\ \text{s.t.} \quad & \sum_{i=1}^4 |p_i|^2 = 4. \end{aligned} \quad (4.28)$$

By the Lagrange multipliers technique, similar to the calculation in Chapter 3, the optimization can be solved. Let

$$F = \frac{1}{8} \left(\sum_{i=1}^2 \left(1 + \frac{1}{2} \rho |p_i|^2\right)^{-4} + \sum_{i=3}^4 \left(1 + \frac{1}{2} \rho |p_i|^2\right)^{-2} \right) + \lambda \left(\sum_{i=1}^4 |p_i|^2 - 4 \right), \quad (4.29)$$

and we will solve the equation

$$\nabla F = 0. \quad (4.30)$$

Assuming $a_i = |p_i|^2$ and omitting some details, we can obtain

$$\begin{aligned} \frac{\partial F}{\partial a_i} = \begin{cases} -\frac{1}{8} \cdot \frac{\rho}{2} \cdot 4 \left(1 + \frac{1}{2} \rho a_i\right)^{-5} + \lambda = 0, & i = 1, 2 \\ -\frac{1}{8} \cdot \frac{\rho}{2} \cdot 2 \left(1 + \frac{1}{2} \rho a_i\right)^{-3} + \lambda = 0, & i = 3, 4 \end{cases} \\ \Rightarrow a_i = \begin{cases} \frac{2}{\rho} \left[\left(\frac{4\rho}{16\lambda} \right)^{\frac{1}{5}} - 1 \right], & i = 1, 2 \\ \frac{2}{\rho} \left[\left(\frac{2\rho}{16\lambda} \right)^{\frac{1}{3}} - 1 \right], & i = 3, 4 \end{cases}. \end{aligned} \quad (4.31)$$

Therefore, as long as we find the suitable λ , the power loading factors are determined.

By substituting a_i for $|p_i|^2$ in the power constraint $\sum_{i=1}^4 |p_i|^2 = 4$, we can get the constraint in terms of the unknown variable λ as follows:

$$\begin{aligned}
& \sum_{i=1}^2 \frac{2}{\rho} \left[\left(\frac{4\rho}{16\lambda} \right)^{\frac{1}{5}} - 1 \right] + \sum_{i=3}^4 \frac{2}{\rho} \left[\left(\frac{2\rho}{16\lambda} \right)^{\frac{1}{3}} - 1 \right] = 4 \\
& \Rightarrow \sum_{i=1}^2 \left(\frac{4\rho}{16\lambda} \right)^{\frac{1}{5}} + \sum_{i=3}^4 \left(\frac{2\rho}{16\lambda} \right)^{\frac{1}{3}} = \frac{4\rho}{2} + 4.
\end{aligned} \tag{4.32}$$

By solving Equation (4.32), we can get λ and then the optimal set of p_i can be obtained.

Compared with the result in spatial multiplexing systems in Chapter 3, we have some notable observations in the results for DSTTD systems. From Equation (4.31), it can be seen that the power loading factors for x_1 and x_2 are identical and so are those for x_3 and x_4 . The reason for this is that $\{x_1, x_2\}$ is encoded by one Alamouti encoder, and $\{x_3, x_4\}$ is encoded by another one. Because of the characteristic of Alamouti encoder, the transmit symbols encoded by the same Alamouti encoder will experience identical channel effects. Therefore, the power loading factors that we obtain will reflect this property which results in $p_1 = p_2$ and $p_3 = p_4$. Besides, from Equation (4.31), it can also be observed that, for any positive λ , the power loading factors have the result that $a_1, a_2 < a_3, a_4$. This is because of the statistical properties of diagonal entries of the \mathbf{R} matrix. The mean of $|R_{11}|$ is smaller than that of $|R_{33}|$ so that the power allocation scheme will allocate more power on the symbols which will be transmitted via the channel $|R_{11}|$.

4.3 Extension of Proposed Optimal Power Allocation Scheme

Since the power loading factors for DSTTD systems with QR receiver is proposed in the previous section, we consider further whether the proposed power allocation scheme can be applied to the multiple space-time transmit diversity (STTD) systems with the QR receiver. We consider a 6×3 triple STTD system with QR successive detection, and the equivalent channel matrix can be expressed as follows:

$$\mathbf{H} = \begin{bmatrix} h_{11} & h_{12} & h_{13} & h_{14} & h_{15} & h_{16} \\ -h_{12}^* & h_{11}^* & -h_{14}^* & h_{13}^* & -h_{16}^* & h_{15}^* \\ h_{21} & h_{22} & h_{23} & h_{24} & h_{25} & h_{26} \\ -h_{22}^* & h_{21}^* & -h_{24}^* & h_{23}^* & -h_{26}^* & h_{25}^* \\ h_{31} & h_{32} & h_{33} & h_{34} & h_{35} & h_{36} \\ -h_{32}^* & h_{31}^* & -h_{34}^* & h_{33}^* & -h_{36}^* & h_{35}^* \end{bmatrix}. \quad (4.33)$$

After QR decomposition, the R matrix is given by

$$\mathbf{R} = \begin{bmatrix} R_{11} & 0 & R_{13} & R_{14} & R_{15} & R_{16} \\ 0 & R_{11} & -R_{14}^* & R_{13}^* & -R_{16}^* & R_{15}^* \\ 0 & 0 & R_{33} & 0 & R_{35} & R_{36} \\ 0 & 0 & 0 & R_{33} & -R_{36}^* & R_{35}^* \\ 0 & 0 & 0 & 0 & R_{55} & 0 \\ 0 & 0 & 0 & 0 & 0 & R_{55} \end{bmatrix}, \quad (4.34)$$

which has a similar structure to the R matrix of QR decomposition of the channel matrix in DSTTD systems. Based on the derivations in Section 4.1, it can be shown that

$2|R_{11}|^2$ has a chi-square distribution with twelve degrees of freedom, and thus the pdf of $|R_{11}|$ is given by

$$p(r_1) = \frac{2r_1^{2(6-1)+1} e^{-r_1^2}}{\Gamma(6)}. \quad (4.35)$$

Although the pdfs of $|R_{33}|$ and $|R_{55}|$ are very difficult to determined directly from

the derivations, we can follow similar approximations in Section 4.1. By means of *dfittool* in MATLAB, the approximations of $2|R_{33}|^2$ and $2|R_{55}|^2$ is shown in Figure 4.3.

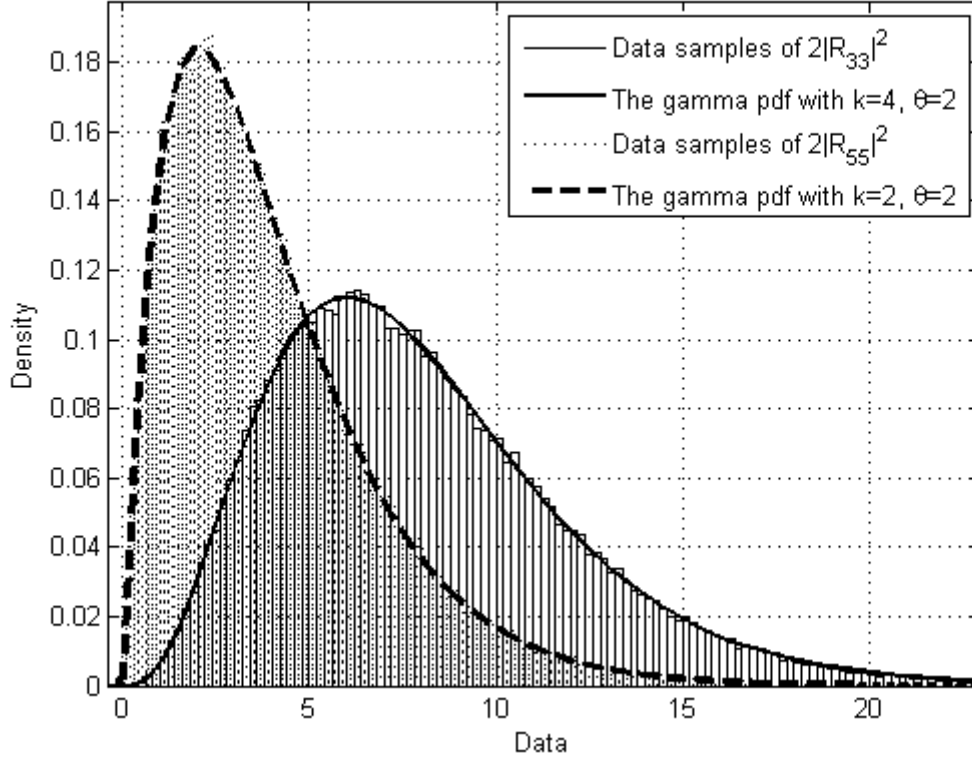


Figure 4.3: Comparisons between $2|R_{33}|^2$, $2|R_{55}|^2$ and the gamma pdfs with $k = 4$, $\theta = 2$, and $k = 2$, $\theta = 2$, respectively

Based on the result of the statistical analysis, following the derivations in Section 4.1, the estimated pdfs of $|R_{33}|$ and $|R_{55}|$ can be given by

$$p(r_3) = \frac{2r_3^{2(6-3)+1}e^{-r_3^2}}{\Gamma(4)}, \quad (4.36)$$

and

$$p(r_5) = \frac{2r_5^{2(6-5)+1}e^{-r_5^2}}{\Gamma(2)}. \quad (4.37)$$

Therefore, the design procedure of the proposed power allocation scheme can be applied for triple STTD systems. Omitting the details of calculation, we can obtain the upper bound for the BER performance without error propagation as follows:

$$\begin{aligned}
\bar{P}_{eL} &= \frac{1}{6} \left[\sum_{i=1}^2 \int_0^{\infty} Q(\sqrt{\rho} |p_i| r_1) \frac{2r_1^{2(6-1)+1} e^{-r_1^2}}{(6-1)!} dr_1 \right. \\
&\quad + \sum_{i=3}^4 \int_0^{\infty} Q(\sqrt{\rho} |p_i| r_3) \frac{2r_3^{2(6-3)+1} e^{-r_3^2}}{(4-1)!} dr_3 \\
&\quad \left. + \sum_{i=5}^6 \int_0^{\infty} Q(\sqrt{\rho} |p_i| r_5) \frac{2r_5^{2(6-5)+1} e^{-r_5^2}}{(2-1)!} dr_5 \right] \quad (4.38) \\
&\leq \frac{1}{12} \left[\sum_{i=1}^2 \left(1 + \frac{1}{2} \rho |p_i|^2\right)^{-6} \right. \\
&\quad \left. + \sum_{i=3}^4 \left(1 + \frac{1}{2} \rho |p_i|^2\right)^{-4} + \sum_{i=5}^6 \left(1 + \frac{1}{2} \rho |p_i|^2\right)^{-2} \right].
\end{aligned}$$

By solving the bound in the above equation, the power loading factors for triple STTD systems can be obtained. It is obvious that the power loading factors for triple STTD systems have similar properties to those for DSTTD systems because of the properties of Alamouti space-time transmit diversity; that is, $p_1 = p_2$, $p_3 = p_4$, and $p_5 = p_6$, and further $p_1, p_2 < p_3, p_4 < p_5, p_6$. Some simulation results are shown and discussed in the next section, and a summary is stated in the end of this chapter.

4.4 Computer Simulations

In the simulations, because the explicit value of λ in Equation (4.32) is difficult to calculate, *fmincon* function in MATLAB is used to find the optimal power loading factors in DSTTD systems. First, considering a 4×2 DSTTD system with QPSK modulation, the evaluations of the upper bound in Equation (4.27) are compared in Figure 4.4. In Figure 4.4, we can see that the upper bound of the lower bound for

overall average BER in DSTTD systems with the proposed power allocation scheme is theoretically improved by about 2 dB at medium-high SNR. To evaluate the real performance of the power allocation scheme, the computer simulation of DSTTD systems with QPSK modulation is shown in Figure 4.5. Although, with power allocation, the BER performances of DSTTD systems with QR receiver is improved, the improvement is around 1 dB which is less than the theoretical result shown in Figure 4.4. Compared with the improvements of power allocation for spatial multiplexing systems in the previous chapter, the gain for DSTTD systems is less than 2dB. This is because that a DSTTD system can be considered as having two parallel transmission links which is equivalent to a 2×2 spatial multiplexing MIMO system. For QR successive detection, the enhancement in the average BER of 2×2 spatial multiplexing systems is less significant than that of 4×4 spatial multiplexing systems. The BER performance comparison of DSTTD systems with different modulation orders are shown in Figure 4.6. It can be seen that when the modulation order increases, the BER performance degrades slightly, and the amount of the improvements by the proposed power allocation schemes decreases as well. The reason is that when the modulation constellation size increases, there will be more nearest neighbors in the constellation. This result is consistent with that for spatial multiplexing MIMO systems. Figure 4.7 shows the BER performances of triple DSTTD systems with QR receiver without and with the power allocation scheme incorporated. It can be seen that the performance is improved by about 1.5 dB at high SNR. This result implies that when the number of transmission links increases, the enhancement induced by the suggested power allocation scheme will be increased.

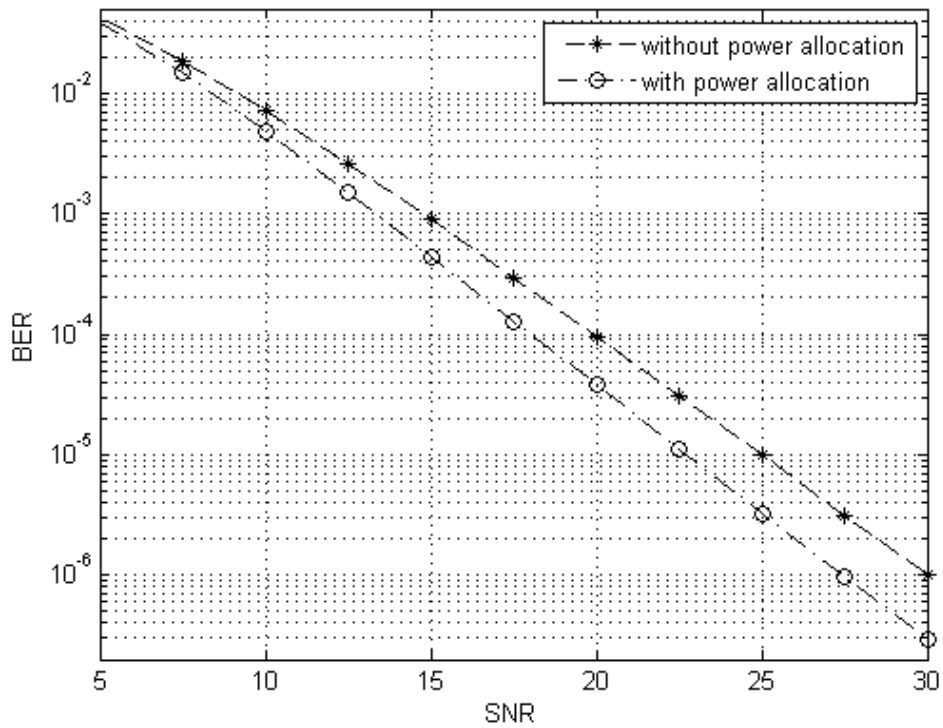


Figure 4.4: Evaluations of upper bounds for the lower bound of average overall BER in DSTTD systems with QPSK modulation

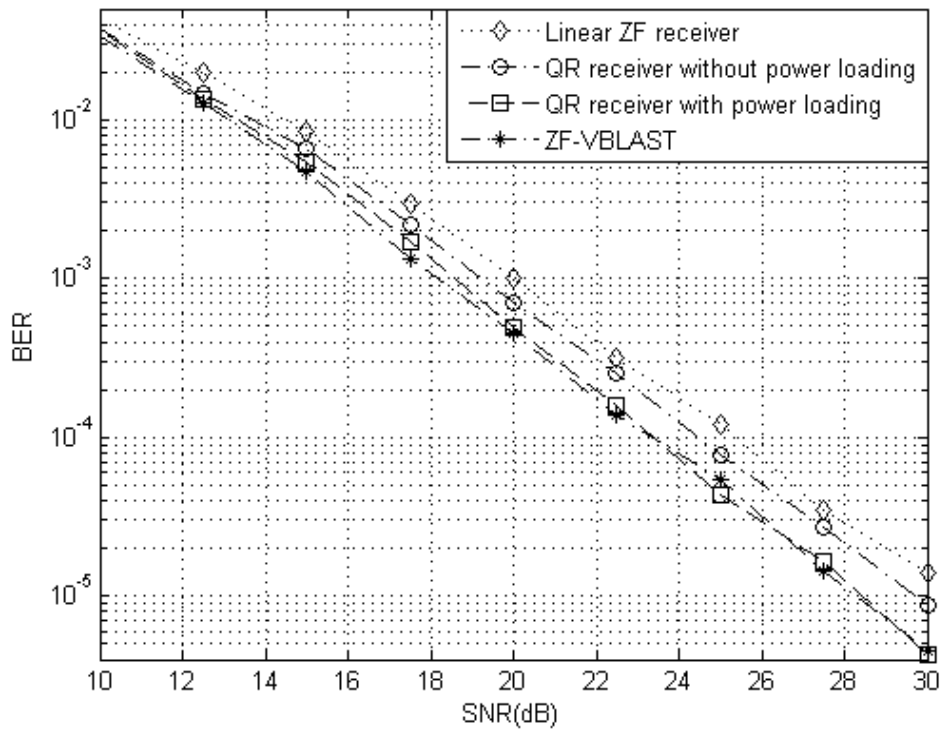


Figure 4.5: Average BER performances of DSTTD systems with different receivers with QPSK modulation

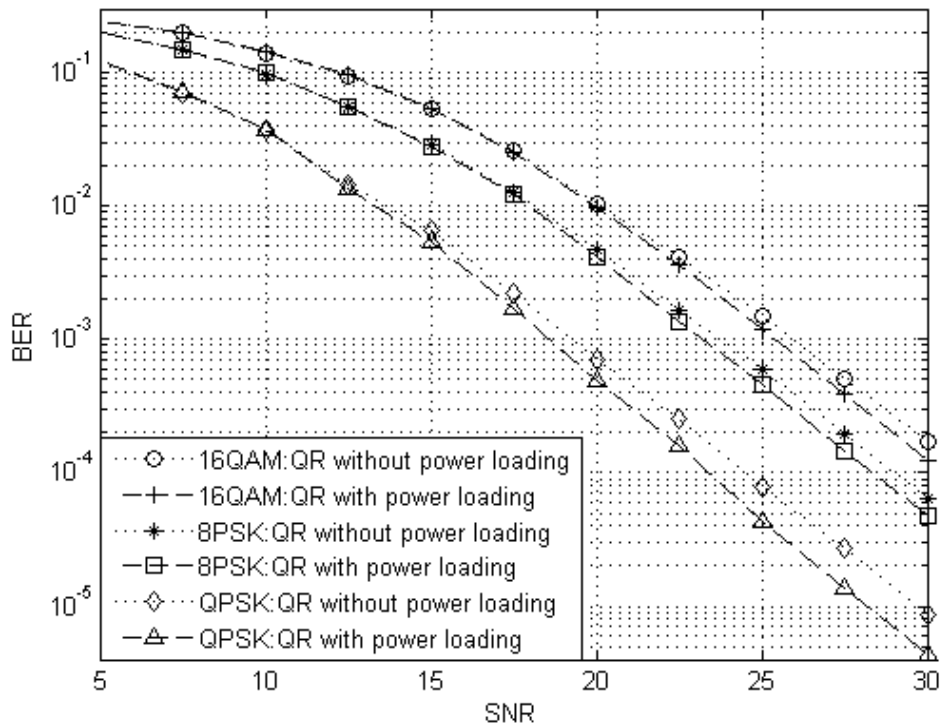


Figure 4.6: Average BER performances of DSTTD systems with the QR receiver with different modulation orders

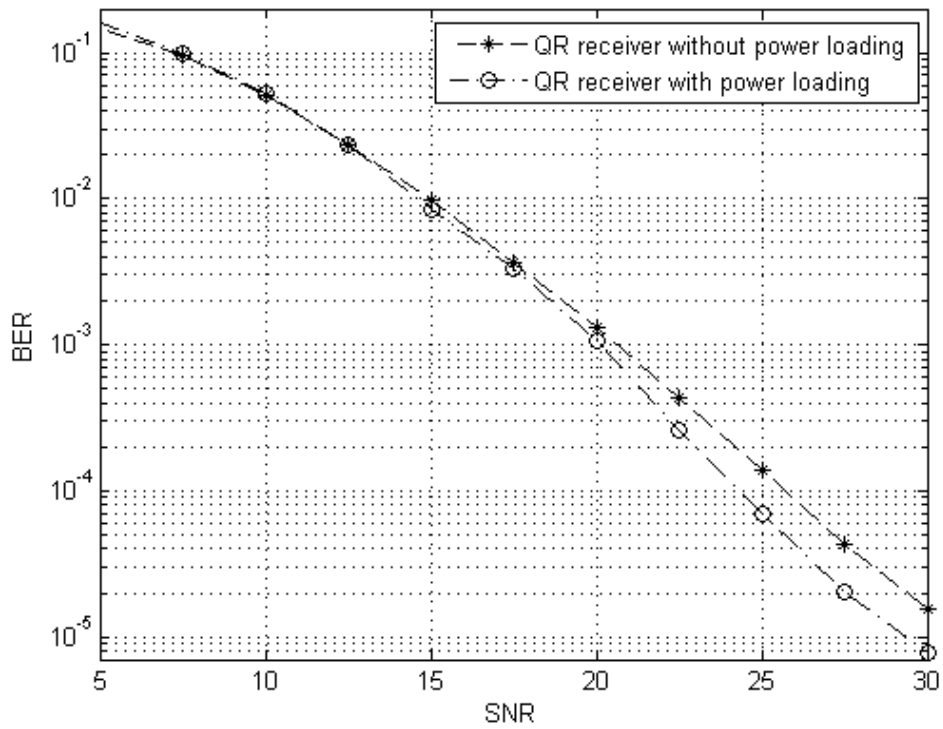


Figure 4.7: Average BER performances of triple STTD systems with the QR receiver

4.5 Summary

In this chapter, we examine the statistical properties of R matrix in QR decomposition for DSTTD systems which is a 2×2 spatial multiplexing MIMO systems combined with Alamouti space-time transmit diversity technique. Although the pdf of $R_{11} = R_{22}$ is easily determined, the exact probability distribution of $R_{33} = R_{44}$ is very difficult to determine. In this case, we model $R_{33} = R_{44}$ as a gamma distribution for $R_{33} = R_{44}$ is related to chi-square random variables, and verify this conjecture with numerical examples. Since the approximated pdf is quite close to the statistic of $R_{33} = R_{44}$, it is possible for us to follow the derivations for spatial multiplexing systems in the previous chapter. The design criterion of the power allocation scheme proposed for DSTTD systems is similar to that for spatial multiplexing systems. Due to the properties of Alamouti space-time transmit diversity, the power loading factors for the transmitted symbols space-time encoded together are identical. From computer simulations, it is shown that the BER performances of DSTTD systems are improved when the power allocation scheme is employed. Furthermore, the proposed power allocation scheme can be extended to multiple STTD systems, since multiple STTD systems can be considered as spatial multiplexing systems with space-time transmit diversity adopted to each sub-stream. The improvements are more significant when the number of transmitted sub-streams increases.

Chapter 5

Conclusion

In this thesis, we consider spatial multiplexing MIMO systems and DSTTD systems over i.i.d. Rayleigh fading channels, and propose a symbol power allocation scheme to minimize the overall average BER performance. In order to achieve a BER performance compromise between linear equalization and joint maximum likelihood (ML) receiver, we propose to adopt QR-based successive detection with proper symbol power allocation. In Chapter 2, we introduce the models of spatial multiplexing systems and DSTTD systems. The QR decompositions of the channel matrices for spatial multiplexing systems and DSTTD systems are given in Section 2.3. The statistical property of diagonal entries of R matrix for spatial multiplexing systems and the special structure of R matrix for DSTTD systems are described. Following that, the detecting procedures for spatial multiplexing systems and DSTTD systems with the QR receiver are demonstrated.

In Chapter 3, the analysis of BER performance of spatial multiplexing systems is given. It is shown that the lower bound for the average BER, although obtained through considering the error propagation free case, is very simple to characterize, and is closely related to the upper bound of the block error rate even when error propagation occurs. Based on this fact and the given statistical property for spatial multiplexing systems stated in Section 2.3.2, considering the robustness to channel variations, an

optimal power allocation scheme for spatial multiplexing systems is proposed to minimize the overall BER averaged with respect to the channel distribution. The simulation results show that the BER performance of spatial multiplexing systems is improved with the proposed power allocation scheme adopted. In Chapter 4, although the distribution of the first entry of the R matrix for DSTTD is determined, the exact distribution of the other entry is very difficult to verify. Observing that the latter mainly consists of chi-square random variables, a natural conjecture is to use the gamma function to estimate its pdf; the result shows that the approximation is quite close. Therefore, the power allocation scheme proposed for spatial multiplexing systems can be extended to DSTTD systems. Computer simulations confirm that the proposed power loading factors can improve the overall average BER performance of DSTTD systems.

The study presented in this thesis has developed a power allocation scheme for spatial multiplexing systems and DSTTD systems by minimizing the overall average BER. We derive the closed-form upper bound of the overall BER averaged with respect to the channel distribution of spatial multiplexing systems. Instead of considering the channel realization, we only need to know the receive SNR to decide which set of power loading factors to adopt. Furthermore, the channel distribution of DSTTD systems or even multiple STTD systems is also approximated so that the design procedure can be applied to multiple STTD systems. As a remark, the proposed power allocation scheme is designed under uncorrelated channels. The distribution of the R matrix may change under correlated channels, and thus the upper bound may have different forms. On the other hand, the space-time code used in DSTTD systems is Alamouti code. It is of interest to see if it is possible to design the power allocation scheme in spatial multiplexing systems with transmitted symbols encoded by more advanced OSTBCs with the QR receiver in a similar way.

Appendix A

Proof of Lemma 2.4

From [19], we follow the proof and revise the error. First, let us define the Hermitian of the channel matrix as follows:

$$\mathbf{H}^H = \begin{bmatrix} \mathbf{H}_1^H & \mathbf{H}_3^H \\ \mathbf{H}_2^H & \mathbf{H}_4^H \end{bmatrix} \triangleq \begin{bmatrix} \mathbf{H}_5 & \mathbf{H}_6 \\ \mathbf{H}_7 & \mathbf{H}_8 \end{bmatrix}. \quad (\text{A.1})$$

We introduce the following two observations which are useful to complete this proof.

1. A unitary matrix \mathbf{Q}_1 with 2×2 Alamouti sub-blocks is shown by

$$\mathbf{Q}_1 = \frac{1}{\sqrt{d_{\mathbf{H}_5} + d_{\mathbf{H}_6}}} \begin{bmatrix} \mathbf{H}_5^H & -\mathbf{H}_6 \\ \mathbf{H}_6^H & \mathbf{H}_6^{-1} \mathbf{H}_5 \mathbf{H}_6 \end{bmatrix}, \quad (\text{A.2})$$

and it satisfies that

$$\begin{bmatrix} \mathbf{H}_5 & \mathbf{H}_6 \end{bmatrix} \frac{1}{\sqrt{d_{\mathbf{H}_5} + d_{\mathbf{H}_6}}} \begin{bmatrix} \mathbf{H}_5^H & -\mathbf{H}_6 \\ \mathbf{H}_6^H & \mathbf{H}_6^{-1} \mathbf{H}_5 \mathbf{H}_6 \end{bmatrix} = \begin{bmatrix} \sqrt{d_{\mathbf{H}_5} + d_{\mathbf{H}_6}} \mathbf{I}_2 & \mathbf{0}_2 \end{bmatrix}. \quad (\text{A.3})$$

2. A unitary matrix \mathbf{Q}_2 with 2×2 Alamouti sub-blocks is shown by

$$\mathbf{Q}_2 = \begin{bmatrix} \mathbf{I}_2 & \mathbf{0}_2 \\ \mathbf{0}_2 & \frac{\mathbf{H}_8^H}{\sqrt{d_{\mathbf{H}_8}}} \end{bmatrix}, \quad (\text{A.4})$$

and it satisfies that

$$\begin{bmatrix} \mathbf{H}_7 & \mathbf{H}_8 \end{bmatrix} \begin{bmatrix} \mathbf{I}_2 & \mathbf{0}_2 \\ \mathbf{0}_2 & \frac{\mathbf{H}_8^H}{\sqrt{d_{\mathbf{H}_8}}} \end{bmatrix} = \begin{bmatrix} \mathbf{H}_7 & \sqrt{d_{\mathbf{H}_8}} \mathbf{I}_2 \end{bmatrix}. \quad (\text{A.5})$$

In the above expressions, $d_{\mathbf{H}_5} = |h_{11}|^2 + |h_{12}|^2$, $d_{\mathbf{H}_6} = |h_{21}|^2 + |h_{22}|^2$, $d_{\mathbf{H}_7} = |h_{13}|^2 + |h_{14}|^2$, and $d_{\mathbf{H}_8} = |h_{23}|^2 + |h_{24}|^2$. It is noted that they are determinants of \mathbf{H}_5 , \mathbf{H}_6 , \mathbf{H}_7 , and \mathbf{H}_8 , respectively. That is,

$$d_{\mathbf{H}_5} = \det(\mathbf{H}_5), \quad d_{\mathbf{H}_6} = \det(\mathbf{H}_6), \quad d_{\mathbf{H}_7} = \det(\mathbf{H}_7), \quad \text{and} \quad d_{\mathbf{H}_8} = \det(\mathbf{H}_8). \quad (\text{A.6})$$

Now we start to derive the proof and assume that there is a matrix with Alamouti

sub-blocks, e.g., $\mathbf{H}^H = \begin{bmatrix} \mathbf{H}_5 & \mathbf{H}_6 \\ \mathbf{H}_7 & \mathbf{H}_8 \end{bmatrix}$. With the observations, we first select

$$\mathbf{Q}_1 = \frac{1}{\sqrt{d_{\mathbf{H}_5} + d_{\mathbf{H}_6}}} \begin{bmatrix} \mathbf{H}_5^H & -\mathbf{H}_6 \\ \mathbf{H}_6^H & \mathbf{H}_6^{-1} \mathbf{H}_5 \mathbf{H}_6 \end{bmatrix}, \quad (\text{A.7})$$

and the first step is given by

$$\begin{aligned} & \begin{bmatrix} \mathbf{H}_5 & \mathbf{H}_6 \\ \mathbf{H}_7 & \mathbf{H}_8 \end{bmatrix} \frac{1}{\gamma} \begin{bmatrix} \mathbf{H}_5^H & -\mathbf{H}_6 \\ \mathbf{H}_6^H & \mathbf{H}_6^{-1} \mathbf{H}_5 \mathbf{H}_6 \end{bmatrix} \\ &= \begin{bmatrix} \gamma \mathbf{I}_2 & \mathbf{0}_2 \\ \frac{1}{\gamma} (\mathbf{H}_7 \mathbf{H}_5^H + \mathbf{H}_8 \mathbf{H}_6^H) & \frac{1}{\gamma} (-\mathbf{H}_7 \mathbf{H}_6 + \mathbf{H}_8 \mathbf{H}_6^{-1} \mathbf{H}_5 \mathbf{H}_6) \end{bmatrix}, \end{aligned} \quad (\text{A.8})$$

where γ is a positive constant defined by $\gamma = \sqrt{d_{\mathbf{H}_5} + d_{\mathbf{H}_6}}$. After that, let us define

the matrix $\mathbf{H}_9 = -\mathbf{H}_7 \mathbf{H}_6 + \mathbf{H}_8 \mathbf{H}_6^{-1} \mathbf{H}_5 \mathbf{H}_6$, and the result will be reduced to

$$\begin{bmatrix} \gamma \mathbf{I}_2 & \mathbf{0}_2 \\ \frac{1}{\gamma} (\mathbf{H}_7 \mathbf{H}_5^H + \mathbf{H}_8 \mathbf{H}_6^H) & \frac{1}{\gamma} (\mathbf{H}_9) \end{bmatrix}. \quad (\text{A.9})$$

Then, we choose

$$\mathbf{Q}_2 = \begin{bmatrix} \mathbf{I}_2 & \mathbf{0}_2 \\ \mathbf{0}_2 & \frac{\mathbf{H}_9^H}{\sqrt{d_{\mathbf{H}_9}}} \end{bmatrix}, \quad (\text{A.10})$$

and the second step is given by

$$\begin{aligned} & \begin{bmatrix} \gamma \mathbf{I}_2 & \mathbf{0}_2 \\ \frac{1}{\gamma} (\mathbf{H}_7 \mathbf{H}_5^H + \mathbf{H}_8 \mathbf{H}_6^H) & \frac{1}{\gamma} (\mathbf{H}_9) \end{bmatrix} \begin{bmatrix} \mathbf{I}_2 & \mathbf{0}_2 \\ \mathbf{0}_2 & \frac{\mathbf{H}_9^H}{\sqrt{d_{\mathbf{H}_9}}} \end{bmatrix} \\ &= \begin{bmatrix} \gamma \mathbf{I}_2 & \mathbf{0}_2 \\ \frac{1}{\gamma} (\mathbf{H}_7 \mathbf{H}_5^H + \mathbf{H}_8 \mathbf{H}_6^H) & \frac{\mathbf{H}_9 \mathbf{H}_9^H}{\gamma \sqrt{d_{\mathbf{H}_9}}} \end{bmatrix}. \end{aligned} \quad (\text{A.11})$$

According to the fundamental properties of Alamouti structure, \mathbf{H}_9 is also an Alamouti block; i.e., $\mathbf{H}_9 \mathbf{H}_9^H = \det(\mathbf{H}_9) \mathbf{I}_2 = d_{\mathbf{H}_9} \mathbf{I}_2$. Therefore, Equation (6.11) can be written as

$$\begin{bmatrix} \gamma \mathbf{I}_2 & \mathbf{0}_2 \\ \frac{1}{\gamma} (\mathbf{H}_7 \mathbf{H}_5^H + \mathbf{H}_8 \mathbf{H}_6^H) & \frac{\sqrt{d_{\mathbf{H}_9}}}{\gamma} \mathbf{I}_2 \end{bmatrix}. \quad (\text{A.12})$$

We arrange the above two processes as follows:

$$\begin{aligned} & \begin{bmatrix} \mathbf{H}_5 & \mathbf{H}_6 \\ \mathbf{H}_7 & \mathbf{H}_8 \end{bmatrix} \frac{1}{\gamma} \begin{bmatrix} \mathbf{H}_5^H & -\mathbf{H}_6 \\ \mathbf{H}_6^H & \mathbf{H}_5^{-1} \mathbf{H}_5 \mathbf{H}_6 \end{bmatrix} \begin{bmatrix} \mathbf{I}_2 & \mathbf{0}_2 \\ \mathbf{0}_2 & \frac{\mathbf{H}_9^H}{\sqrt{d_{\mathbf{H}_9}}} \end{bmatrix} \\ &= \begin{bmatrix} \gamma \mathbf{I}_2 & \mathbf{0}_2 \\ \frac{1}{\gamma} (\mathbf{H}_7 \mathbf{H}_5^H + \mathbf{H}_8 \mathbf{H}_6^H) & \frac{1}{\gamma} (-\mathbf{H}_7 \mathbf{H}_6 + \mathbf{H}_8 \mathbf{H}_6^{-1} \mathbf{H}_5 \mathbf{H}_6) \end{bmatrix} \begin{bmatrix} \mathbf{I}_2 & \mathbf{0}_2 \\ \mathbf{0}_2 & \frac{\mathbf{H}_9^H}{\sqrt{d_{\mathbf{H}_9}}} \end{bmatrix} \\ &= \begin{bmatrix} \gamma \mathbf{I}_2 & \mathbf{0}_2 \\ \frac{1}{\gamma} (\mathbf{H}_7 \mathbf{H}_5^H + \mathbf{H}_8 \mathbf{H}_6^H) & \frac{\mathbf{H}_9 \mathbf{H}_9^H}{\gamma \sqrt{d_{\mathbf{H}_9}}} \end{bmatrix} = \begin{bmatrix} \gamma \mathbf{I}_2 & \mathbf{0}_2 \\ \frac{1}{\gamma} (\mathbf{H}_7 \mathbf{H}_5^H + \mathbf{H}_8 \mathbf{H}_6^H) & \frac{\sqrt{d_{\mathbf{H}_9}}}{\gamma} \mathbf{I}_2 \end{bmatrix}. \end{aligned} \quad (\text{A.13})$$

Let us combine \mathbf{Q}_1 and \mathbf{Q}_2 as

$$\mathbf{Q} = \mathbf{Q}_1 \mathbf{Q}_2 = \frac{1}{\sqrt{d_{\mathbf{H}_5} + d_{\mathbf{H}_6}}} \begin{bmatrix} \mathbf{H}_5^H & -\mathbf{H}_6 \\ \mathbf{H}_6^H & \mathbf{H}_6^{-1} \mathbf{H}_5 \mathbf{H}_6 \end{bmatrix} \begin{bmatrix} \mathbf{I}_2 & \mathbf{0}_2 \\ \mathbf{0}_2 & \frac{\mathbf{H}_9^H}{\sqrt{d_{\mathbf{H}_9}}} \end{bmatrix}, \quad (\text{A.14})$$

and define the lower triangular matrix

$$\mathbf{L} = \begin{bmatrix} \gamma \mathbf{I}_2 & \mathbf{0}_2 \\ \frac{1}{\gamma} (\mathbf{H}_7 \mathbf{H}_5^H + \mathbf{H}_8 \mathbf{H}_6^H) & \frac{\sqrt{d_{\mathbf{H}_9}}}{\gamma} \mathbf{I}_2 \end{bmatrix}. \quad (\text{A.15})$$

The result (6.13) can thus be translated into $\mathbf{H}^H \mathbf{Q} = \mathbf{L}$. We rewrite $\mathbf{H}^H \mathbf{Q} = \mathbf{L}$ as

$(\mathbf{H}^H \mathbf{Q})^H = \mathbf{Q}^H \mathbf{H} = \mathbf{L}^H = \mathbf{R}$ and obtain $\mathbf{H} = \mathbf{Q} \mathbf{R}$ equivalently, where

$$\mathbf{Q} = \frac{1}{\sqrt{d_{\mathbf{H}_5} + d_{\mathbf{H}_6}}} \begin{bmatrix} \mathbf{H}_5^H & -\mathbf{H}_6 \\ \mathbf{H}_6^H & \mathbf{H}_6^{-1} \mathbf{H}_5 \mathbf{H}_6 \end{bmatrix} \begin{bmatrix} \mathbf{I}_2 & \mathbf{0}_2 \\ \mathbf{0}_2 & \frac{\mathbf{H}_9^H}{\sqrt{d_{\mathbf{H}_9}}} \end{bmatrix}, \quad (\text{A.16})$$

and

$$\begin{aligned} \mathbf{R} &= \begin{bmatrix} \gamma \mathbf{I}_2 & \mathbf{0}_2 \\ \frac{1}{\gamma} (\mathbf{H}_7 \mathbf{H}_5^H + \mathbf{H}_8 \mathbf{H}_6^H) & \frac{\sqrt{d_{\mathbf{H}_9}}}{\gamma} \mathbf{I}_2 \end{bmatrix}^H = \begin{bmatrix} \gamma \mathbf{I}_2 & \frac{1}{\gamma} (\mathbf{H}_7 \mathbf{H}_5^H + \mathbf{H}_8 \mathbf{H}_6^H)^H \\ \mathbf{0}_2 & \frac{\sqrt{d_{\mathbf{H}_9}}}{\gamma} \mathbf{I}_2 \end{bmatrix} \\ &= \begin{bmatrix} \sqrt{\det(\mathbf{H}_5) + \det(\mathbf{H}_6)} \mathbf{I}_2 & \frac{1}{\sqrt{\det(\mathbf{H}_5) + \det(\mathbf{H}_6)}} (\mathbf{H}_5 \mathbf{H}_7^H + \mathbf{H}_6 \mathbf{H}_8^H) \\ \mathbf{0}_2 & \frac{\sqrt{\det(\mathbf{H}_9)}}{\sqrt{\det(\mathbf{H}_5) + \det(\mathbf{H}_6)}} \mathbf{I}_2 \end{bmatrix}. \end{aligned} \quad (\text{A.17})$$

The proof is completed and it is easy to check that \mathbf{Q} preserves the structure of 2×2 Alamouti's sub-blocks and the right upper part of \mathbf{R} is an Alamouti block as well.

It is obvious that the diagonal entries of \mathbf{R} are related to the determinants of the partitioned matrices. Because \mathbf{Q} is a unitary matrix, the determinant of \mathbf{Q} is equal to one. It is easy to see that the determinant of \mathbf{H} is equal to the determinant of \mathbf{R} , which is the product of the diagonal entries of \mathbf{R} since \mathbf{R} is an upper triangular matrix. Then we calculate the determinant of \mathbf{R} , and find the following relationship

between \mathbf{R} and \mathbf{H}_9 :

$$\det(\mathbf{H}) = \det(\mathbf{R}) = \gamma^2 \left(\frac{\sqrt{d_{\mathbf{H}_9}}}{\gamma} \right)^2 = d_{\mathbf{H}_9} = \det(\mathbf{H}_9) \quad (\text{A.18})$$

From the definition of (6.1), we have the relations as follows:

$$\begin{aligned} \det(\mathbf{H}_5) &= \det(\mathbf{H}_1^H) = \det(\mathbf{H}_1), \quad \det(\mathbf{H}_6) = \det(\mathbf{H}_3^H) = \det(\mathbf{H}_3), \\ \det(\mathbf{H}_7) &= \det(\mathbf{H}_2^H) = \det(\mathbf{H}_2), \quad \text{and} \quad \det(\mathbf{H}_8) = \det(\mathbf{H}_4^H) = \det(\mathbf{H}_4). \end{aligned} \quad (\text{A.19})$$

Finally, we can rewrite \mathbf{R} as

$$\mathbf{R} = \begin{bmatrix} \sqrt{\det(\mathbf{H}_1) + \det(\mathbf{H}_3)} \mathbf{I}_2 & \frac{1}{\sqrt{\det(\mathbf{H}_1) + \det(\mathbf{H}_3)}} (\mathbf{H}_1^H \mathbf{H}_2 + \mathbf{H}_3^H \mathbf{H}_4) \\ \mathbf{0}_2 & \frac{\sqrt{\det(\mathbf{H})}}{\sqrt{\det(\mathbf{H}_1) + \det(\mathbf{H}_3)}} \mathbf{I}_2 \end{bmatrix}. \quad (\text{A.20})$$



Bibliography

- [1] G. J. Foschini, "Layered space-time architecture for wireless communication in a fading environment when using multiple antennas," *Bell Labs Technical Journal*, vol. 1, pp. 41-59, Autumn 1996.
- [2] G. J. Foschini and M. J. Gans, "On limits of wireless communications in a fading environment when using multiple antennas," *Wireless Personal Communications*, vol. 6, pp. 311-335, Mar. 1998.
- [3] V. Tarokh, N. Seshadri, and A. R. Calderbank, "Space-time codes for high data rate wireless communication: Performance analysis and code construction," *IEEE Trans. Inform. Theory*, vol. 44, no. 2, pp. 744-765, Mar. 1998.
- [4] S. M. Alamouti, "A simple transmitter diversity scheme for wireless communications," *IEEE J. Select. Areas Commun.*, vol. 16, pp. 1451-1458, Oct. 1998.
- [5] 3GPP TDoc R1-010458, Texas Instruments, "Double STTD scheme for HSDPA systems with four transmit antennas: Link level simulations," RAN1#20, Busan, Korea, May 21-25, 2001.
- [6] E. N. Onggosanusi, A. G. Dabak, and T. M. Schmidl, "High rate space-time block coded scheme: Performance and improvement in correlated fading channels," *Proc. of IEEE Wireless Communications and Networking Conference*, vol. 1, pp. 194-199, Mar. 2002.
- [7] S. Shim, K. Kim, and C. Lee, "An efficient antenna shuffling scheme for a DSTTD system," *IEEE Commun. Lett.*, vol. 9, no. 2, pp. 124-126, Feb. 2005.
- [8] A. Scaglione, P. Stoica, S. Barbarossa, G. Giannakis, and H. Sampath, "Optimal designs for space-time linear precoders and decoders," *IEEE Trans. Signal Process.*, vol. 50, no. 5, pp. 1051-1064, May 2002.
- [9] H. Zhuang, L. Dai, S. Zhou, and Y. Yao, "Low complexity per-antenna rate and power control approach for closed-loop V-BLAST," *IEEE Trans. Commun.*, vol. 51, no.11, pp. 1783-1787, Nov. 2003.
- [10] R. Kalbasi, D. D. Falconer, and A. H. Banihashemi, "Optimum power allocation

- for a V-BLAST system with two antennas at the transmitter,” *IEEE Trans. Commun.*, vol. 9, no. 9, pp. 826-828, Sep. 2005.
- [11] N. Prasad and M. K. Varanasi, “Analysis of decision feedback detection for MIMO Rayleigh-fading channels and optimization of power and rate allocation,” *IEEE Trans. Inform. Theory*, vol. 50, no. 6, pp. 1009-1025, Jun. 2004.
- [12] H. Kim and H. Park, “Efficient successive interference cancellation algorithms for the DSTTD system,” *Proc. IEEE PIMRC*, pp. 62-66, Sep. 2005.
- [13] J. Ham, S. Shim, K. Kim, and C. Lee, “A simplified adaptive modulation scheme for D-STTD systems with linear receivers,” *IEEE Commun. Lett.*, pp. 1049-1051, Dec. 2005.
- [14] H. Kim, T. Kim, I. Eo, and H. Park, “Performance analysis of a DSTTD system with decision-feedback detection,” *Proc. IEEE ICASSP*, pp. 749-752, May 2006.
- [15] Z. Yan, K.M. Wong, and Z. Q. Luo, “Optimal diagonal precoder for multiantenna communication systems,” *IEEE Trans. Signal Process.*, vol. 53, no. 6, pp. 2089-2100, Jun. 2005.
- [16] P. W. Wolnianaky, G. J. Foschini, G. D. Golden, and R. A. Valenzuela, “V-BLAST: An architecture for realizing very high data rates over rich-scattering wireless channels,” *Proc. IEEE ISSSE-98*, Italy, pp. 295-300, Sep. 1998.
- [17] A. Wittneben, “Base station modulation diversity for digital simulcast,” *Proc. IEEE VTC*, pp. 505-511, May 1993.
- [18] N. Seshadri and J. H. Winters, “Two signaling schemes for improving the error performance of frequency-division-duplex transmission systems using transmitter antenna diversity,” *Int. J. Wireless Inform. Networks*, vol. 1, no. 1, 1994
- [19] A. H. Sayed, W. M. Younis, and A. Tarighat, “An invariant matrix structure in multiantenna communications,” *IEEE Trans. Signal Process.*, vol. 12, no. 11, pp. 749-752, Nov. 2005.
- [20] R. J. Muirhead, *Aspects of Multivariate Statistical Theory*. New York: Wiley, 1982.
- [21] J. G. Proakis, *Digital Communications*, Boston, MA: McGraw-Hill, 2001.
- [22] A. M. Tulino and S. Verdú, “Random matrix theory and wireless communications,” *Foundations and Trends in Commun. and Inf. Theory*, vol. 1, no. 1, pp. 1-182, 2004.